catalysts

MDPI

Article

Co-Assembled Supported Catalysts: Synthesis of Nano-Structured Supported Catalysts with Hierarchic Pores through Combined Flow and Radiation Induced Co-Assembled Nano-Reactors

Galip Akay [1,2]

[1] Faculty of Science and Arts, Canik Basari University, 55080 Samsun, Turkey; galip.akay1@gmail.com; Tel.: +90-545-650-2055 or +44-788-751-2446

[2] Department of Chemical Engineering and Advanced Materials, Newcastle University, Newcastle upon Tyne NE1 7RU, UK

Academic Editor: Keith Hohn

Received: 9 March 2016; Accepted: 9 May 2016; Published: 28 May 2016

Abstract: A novel generic method of silica supported catalyst system generation from a fluid state is presented. The technique is based on the combined flow and radiation (such as microwave, thermal or UV) induced co-assembly of the support and catalyst precursors forming nano-reactors, followed by catalyst precursor decomposition. The transformation from the precursor to supported catalyst oxide state can be controlled from a few seconds to several minutes. The resulting nano-structured micro-porous silica supported catalyst system has a surface area approaching 300 m^2/g and X-ray Diffraction (XRD)-based catalyst size controlled in the range of 1–10 nm in which the catalyst structure appears as lamellar sheets sandwiched between the catalyst support. These catalyst characteristics are dependent primarily on the processing history as well as the catalyst (Fe, Co and Ni studied) when the catalyst/support molar ratio is typically 0.1–2. In addition, Ca, Mn and Cu were used as co-catalysts with Fe and Co in the evaluation of the mechanism of catalyst generation. Based on extensive XRD, Scanning Electron Microscopy (SEM) and Transmission Electron Microscopy (TEM) studies, the micro- and nano-structure of the catalyst system were evaluated. It was found that the catalyst and silica support form extensive 0.6–2 nm thick lamellar sheets of 10–100 nm planar dimensions. In these lamellae, the alternate silica support and catalyst layer appear in the form of a bar-code structure. When these lamellae structures pack, they form the walls of a micro-porous catalyst system which typically has a density of 0.2 g/cm^3. A tentative mechanism of catalyst nano-structure formation is provided based on the rheology and fluid mechanics of the catalyst/support precursor fluid as well as co-assembly nano-reactor formation during processing. In order to achieve these structures and characteristics, catalyst support must be in the form of silane coated silica nano-particles dispersed in water which also contains the catalyst precursor nitrate salt. This support-catalyst precursor fluid must have a sufficiently low viscosity but high elastic modulus (high extensional viscosity) to form films and bubbles when exposed to processing energy sources such as microwave, thermal, ultra-sound or UV-radiation or their combination. The micro-to-nano structures of the catalyst system are essentially formed at an early stage of energy input. It is shown that the primary particles of silica are transformed to a proto-silica particle state and form lamellar structures with the catalyst precursor. While the nano-structure is forming, water is evaporated leaving a highly porous solid support-catalyst precursor which then undergoes decomposition to form a silica-catalyst oxide system. The final catalyst system is obtained after catalyst oxide reduction. Although the XRD-based catalyst size changes slightly during the subsequent heat treatments, the nano-structure of the catalyst system remains substantially unaltered as evaluated through TEM images. However, if the catalyst preparation is carried out without film formation, the XRD-based catalyst size increases substantially by a factor of 2–8, with no significant alteration in surface area.

Keywords: catalyst synthesis; catalysts with hierarchic pores; co-assembled catalysts; co-assembly; co-assembled nano-reactors; flow induced assembly; heterogeneous catalysis; nano-reactors; nano-structured catalysts; process intensification; radiation induced assembly; self-assembly; silica supported catalysts; supported catalysts

1. Introduction

1.1. Heterogeneous Catalysts and Catalyst Support

Heterogeneous chemical catalysis is a very important and well known technology. In order to enhance the activity, selectivity and efficiency of the catalysts, they are often supported or chemically bound on porous support materials with a very high surface area. Highly porous solids such as zeolites, carbon, silica or alumina and more recently nanotubes/rods or mesoporous silica have been used for this purpose. Excellent reviews of the subject are available [1,2].

The catalyst activity is strongly dependent on the size of the catalyst nanoparticles which therefore need to be minimized during processing. There are several strategies available to achieve a small catalyst size [1–7]. Relevant to this study, the methods include processing under a nitric oxide atmosphere during the decomposition of the catalyst precursor nitrate salt [4,7] or physical agitation [7].

Once supported on a porous material, the catalyst is activated, the extent of which is dependent on the catalyst size, catalyst composition and interaction with the support, as well as service conditions after activation. Apart from catalyst poisoning, the main reason for activity decay is the growth of metal catalyst particles. Catalyst agglomeration/size enlargement is caused by blockage of the pores of the support material, inaccessibility of all the pores to the catalyst precursor molecules and the calcination process at high temperatures during catalyst activation. In order to mitigate catalyst size enlargement, it is also possible to control 3D distribution of the nanoparticles [4].

Although the catalyst size and surface area are affected by the surface area of the support, catalyst loading on the support is mainly on the outer surface of the support and the accessibility of the catalyst particles to the reactants is not uniform. Once again, catalysts on the support surface are the primary contributors to the reactions. In order to overcome these drawbacks, porous catalyst systems in particulate form have been designed thus allowing mass transfer with a diffusion path of micro-to- submicron levels instead of millimeter scale [8,9].

1.2. Monolithic Reactors for Catalysis

In order to enhance the interfacial surface area for heat and mass transfer, porous monoliths have also been used as a catalyst support [10–12]. These so called structured catalysts in the form of monoliths with a hierarchic pore structure also provide convective heat and mass transfer through the interconnecting holes whereas conductive processes take place at the walls. Such metallic monoliths are available commercially under the trade names of Retimet or Recimet [13]. These monoliths have a high porosity (*ca.* 80%) but suffer from a relatively low surface area (*ca.* 0.1 m^2/g) and large pore size (*ca.* 500–50 μm). Recently, nanostructured microporous metal foams with a bimodal pore size distribution at *ca.* 10 μm and *ca.* 10 nm have been produced [12] using flow induced electroless metal deposition on microporous templates, followed by calcination when nanostructure was formed. Such monoliths can be used as catalytic reactors [12].

The walls of commercially available monoliths (such as Retimet ®) [13] can be catalyzed and used as catalytic reactors. This is achieved by wash coating of the walls followed by catalyst reduction. Large pores (or channels) provide convective mass transfer while the surface coated catalyst provides the catalytic transformation. However, in these systems, catalyst loading is low and is liable to erosion and the interfacial area for mass transfer is low.

1.3. Confinement Phenomenon and Reactions in Micro- and Nano-Scale Reactors

Micro-porous materials with controlled pore size, pore connectivity and biochemical activity also provide a suitable means of investigating chemical or biochemical processes within a confined environment which appears to yield several phenomena [14–17]. Such size dependent confinement phenomena [17] can be used in process intensification [17] to achieve faster and more efficient chemical/biochemical conversions [14–17].

The advantages of micro-scale synthetic confinement system/reactors include ease of fabrication of micro-reactors, control of their structure, monitoring and visualization by scanning electron microscopy which is invaluable in determining the mechanism of the prevailing processes.

Confinement phenomena at nano-scale has been known for a long time in nature and surfactants. The research into the formation and applications of nano-reactors/structures is gaining momentum and recent reviews are available in chemical or biochemical systems [18–21].

In macro- and micro-reactors, the so called "reactor" is fabricated in the first instance and simultaneous momentum, heat and mass transfer in 3-dimension can be controlled and monitored well. In the currently available nano-reactor systems, the control of these variables is severely restricted, especially in biological systems, and the only important transport process is mass transfer by diffusion as self-assembled nano-reactor formation is spontaneous. Therefore, momentum (flow) and heat transfer do not have any significant role in both the formation of nano-reactors and their operation.

In micro-reactors, mass transfer is still strongly influenced by the prevailing momentum and heat transfer, although the interactions between flow, fluid micro-structure (in surfactant or polymeric or dispersed systems) and fluid-wall interactions influence the chemical reactions. These effects can be described as "physico-chemical flow effects" and include for example mechano-chemical reactions, flow induced phase transfer, flow induced diffusion; flow induced phase inversion and flow induced electroless deposition [12,17,22].

1.4. An Alternative Method of Nano-Reactor Formation and Reactions at Nano-Scale

Another approach to nano-reactor formation and reaction within them is to form the nano-reactors through the simultaneous application of momentum, heat and mass transfer, followed by the initiation of the desired reaction. For any practical application of this approach, these processes must be very rapid but yet controllable, capable of being scaled-up and they should provide some processing and thermodynamic advantages such as low temperature and pressure operations and high selectivity and product quality.

In this study, we present a generic technique of obtaining nano-reactors in the form of co-assembled solid films which could be considered as nano-scale monoliths. These reactors already contain the reactants. The energy source required for self-assembly can also be used to initiate the desired reaction. Here, we use thermal, micro-wave or solar radiation (or UV) for self-assembly and reaction. The resulting product is in fact a supported catalyst with hierarchic pore structure having a novel nano-structure, controllable small (as low as a nanometer) crystallite size, high surface area and catalyst loading (*ca.* 0.7 mole fraction).

2. Experimental

2.1. Materials

2.1.1. Catalyst Precursors

Catalyst precursors used in this study were d-metal nitrates; $Fe_2(NO_3)_3 \cdot 6H_2O$, $Co(NO_3)_2 \cdot 6H_2O$, $Ni(NO_3)_2 \cdot 6H_2O$; $Cu(NO_3)_2 \cdot 3H_2O$; and $Mn(NO_3)_2 \cdot 6H_2O$ as well as $Ca(NO_3)_2 \cdot 4H_2O$ (all analytical grade). They were all supplied by Sigma Aldrich (Dorset, England).

2.1.2. Support Precursors

Precipitated silica with particle size of 7 nm (Aerosil EA 380) was provided by Degussa/Evonik, Essen, Germany.

Epoxy silane (γ-Glycidoxypropyltrimethoxysilane) coated silica dispersion was supplied by AkzoNobel (Bohus, Sweden) in the form of a 30 wt % dispersion under the trade name of Bindzil 30CC. The size of the silica particles was 7 nm. Despite its very large silica loading, its viscosity is low, thus enabling its processing using standard laboratory equipment.

Macro-porous metal foam (Grade 4753) was supplied by Recemat International, Krimpen, The Netherlands. It had 0.4 mm average pore size, 1.6 mm thickness, 86% porosity and 0.1 m^2/g specific surface area. This material is used as a confinement environment in the preparation of silica supported cobalt catalyst.

2.2. Analytical Methods

2.2.1. Interfacial Rheometer

Both the interfacial tension and the bulk flow characteristics of the coated silica dispersion were measured using an Interfacial Rheometer supplied by Biolin Scientific (Helsinki, Finland). This is an optical technique based on oscillating pendant drop [23].

A drop of the liquid is generated at the end of a capillary and its volume is oscillated sinusoidally while recording the image of the oscillating drop from which the variation of the drop surface area was computed and recorded as a function of time and frequency. Using the theory developed by Miller *et al.* [23] the rheological properties of the liquid were computed, giving the viscous (loss) modulus, E′ and elastic (storage) modulus, E″. This optical rheometer also provides surface tension as a function of time.

2.2.2. Thermogravimetric Analysis (TGA)

A Perkin Elmer thermogravimetric analyzer was used to follow the decomposition of catalyst precursor solutions (nitrate). An approximately 10 mg sample was used. Starting from room temperature, the sample was heated at a rate of 10 °C/min to reach 500 °C at atmospheric pressure under flowing nitrogen.

2.2.3. Nitric Oxide Analysis

A CDS Analytical Inc., (Oxford, PA, USA) pyrolyser (Pyroprobe 5000 Series) was used for the decomposition of cobalt nitrate solution and coated silica dispersion containing the same amount (1 M) of cobalt nitrate. The temperature of the pyrolysis chamber was increased to 1300 °C from room temperature in two stages. In stage-1, the rate of temperature increase was 2 °C/min up to 220 °C. In stage 2, the rate of increase was 20 °C/min from 220 °C up to 1300 °C. After cooling, the emerging gases were directed continuously to an Agilent Micro-GC Gas Analyzer (Bouldon, Tyne and Wear, UK) to determine nitric oxide concentration in the pyrolysis gases.

2.2.4. BET Surface Area Analysis

A Beckman-Coulter SA 3100 analyzer (Beckman Coulter (UK) Ltd., High Wycombe, England) was used to measure the surface area of the catalyst systems based on Brunauer-Emmett-Teller (BET) theory. This instrument uses the gas sorption technique to obtain the surface area and pore size distributions at room temperature using helium. Specific surface area of the metallized monoliths were calculated after measuring the bulk density of the samples in order to compare these materials with commercially available porous metals.

2.2.5. Scanning Electron Microscopy (SEM) and Energy Dispersive X-ray (EDX) Analysis

The scanning electron microscope used in the present work was an Environmental Scanning Electron Microscopy (XL30 ESEM-FEG) (Philips Electronics UK Ltd, Guildford, UK) fitted with a Rontec Quantax system for Energy Dispersive X-ray (EDX) analysis to obtain local atomic concentration of various elements in metallic samples after heat treatment. Since the metallic samples were conductive, they were not coated.

High magnification SEM imaging were carried out using a Joel JSM-7001F Field Emission SEM (Tokyu, Japan) fitted with a X-Max 80 mm^2 EDX detector manufactured by Oxford Instruments (Oxford, UK). At high magnifications (*i.e.*, >50 k magnification), the samples were gold coated.

2.2.6. Transmission Electron Microscopy (TEM) Analysis

The fine structure of the catalyst samples were analyzed with a Philips CM100 Transmission Electron Microscope (TEM) (Guildford, UK) and the images were collected using an AMT CCD camera (Woburn, Massachusetts, MA, USA).

2.2.7. X-Ray Diffraction (XRD) Analysis

The X-ray Diffraction (XRD) equipment was a PANalytical X'Pert Pro diffractometer (Almelo, The Netherlands), fitted with an X'Celerator (Almelo, The Netherlands). The X'Celerator is a relatively new attachment to the X'Pert and has the effect of giving a good quality pattern in a fraction of the time of the traditional diffractometer. XRD was not only used to identify the phase structures of the catalysts but also to estimate the crystal size using the Scherrer equation [24,25].

2.3. Processing Equipment and Supported Catalyst Preparation

Silica supported catalysts were prepared by using 3 different methods in order to determine the mechanism of supported catalyst formation. In these experiments we have either used uncoated silica particles (size 7 nm) or coated silica particles dispersed in water (*i.e.*, Bindzil 30CC) with 7 nm particle size. Although the coated silica solution was highly concentrated (30 wt % silica) its viscosity was low (10 cP). It is therefore possible to mix the appropriate amount of catalyst salt with the coated silica dispersion directly, to obtain a clear solution. On the other hand, at the same silica concentration level, uncoated silica in water essentially forms a highly viscous paste thus making the use of a high torque mixer (such as the equipment used herein) essential. The processing equipment and the method used in this study are described below.

2.3.1. Haake Mixer/Rheometer

A Haake Rheocord Torque Rheometer 9000 (Supplied by Thermo Electron Corporation, Waltham, Massachusetts, USA) was used as a mixing device for the highly viscous paste of silica support (using uncoated silica) with the catalyst precursor. It was also used to demonstrate the mechanism of flow induced supported catalyst formation when coated silica was used as the support.

Haake Rheocord Torque Rheometer consists of three basic components, a horizontally mounted, heavy duty motor drive together with a torque sensor which is attached to mixing heads, two 2 sigma rotary blades. These two blades rotate at 2:1 ratio speeds within adjoining cylindrical cavities of a mixer chamber, and they produce a relatively high shear rate (typically 100 s^{-1}), and a complex deformation pattern which involves alternate shearing and relaxation at the mixer wall and rotor; the clearance between them being *ca.* 0.2 mm. Details of the Haake Rheometer and its use in the present mode are available [22].

2.3.2. GAP-Agglomerator

GAP Agglomerator was designed and developed by the author and assigned to GAP Technologies Ltd. (London, UK). It is essentially a continuous processing form of the Haake Rheometer described

above (2.3.1). Here we use this intensified agglomerator [17,26] in order to obtain agglomerated silica supported catalysts, as supported catalysts are often used in agglomerated form. This equipment was purpose built and utilized in the conversion of liquids into agglomerated powder after going through a highly viscous paste like phase. It consists of a rotor and stator disks with cavities to mix and transfer/pump liquids or solids or their mixtures. The details of the basic technique and equipment is available [17,26].

2.3.3. Microwave Reactors

Experiments for screening purposes were conducted using a kitchen microwave oven supplied by Panasonic UK (Bracknell, UK). It had a fixed power rating of 1 kW.

A Milestone Ethos-1 microwave system (supplied by Milestone Srl, Sorisole (BG), Italy) was used in the assessment of the mechanism of catalyst generation. It had a dual magnetron system with a pyramid-shaped diffuser for homogeneous microwave distribution. The maximum power rating was 1500 W delivering power controlled via a microprocessor in 1 W increment either continuously or pulsed microwave emission. The interior of the reactor was PTFE coated against acid/organic solvents. Air flow through the reactor ensures fast cooling of the reactor. Temperature of the reactor chamber as well as the reacting mixture was recorded. This microwave reactor was fitted with a round bottom flask which had a temperature probe and gas-exit. In addition, it was also possible to insert an ultra-sound probe to superimpose microwave and ultra-sound radiations.

Microwave irradiation at elevated temperatures was carried out using a Milestone Microwave Pyro system supplied by Milestone Srl, Sorisole (BG), Italy. This reactor was also supplied by Milestone Slr, Italy. It is similar to the Milestone Etos-1 system described above, except that the temperature of the reactor could by increased to 800 °C during microwave irradiation.

2.3.4. UV-Radiation Chamber

An agricultural growth cabinet (Fitotron Model SGC097.CPX.F) manufactured by Weiss Gallenkamp (Loughborough, UK) was used as the UV-radiation source. This agricultural growth cabinet simulates solar radiation [15]. The radiation level of the growth cabinet was set at the maximum giving a radiation dose at LUX = 82,000 lx, as measured by a digital illuminance meter Iso-Tech, type ILM 1332A, supplied by RS Components Ltd (Corby, UK). The temperature of the cabinet was 25 °C and the relative humidity was kept at 50%.

3. Results

Although the composition and processing history associated with each sample described in the figures are summarized, we have used the following notation in the description of the samples:

M/Si = 1/x: Catalyst (M = Ni, Co, Fe) and silica support molar ratio is [M]/[Si] =1/x
M/N/Si = 1/y/x: Catalyst (M = Ni, Co, Fe), co-catalyst (N = Ca, Mn, Cu) and silica support molar ratio is [M]/[N]/[Si] =1/y/x
Mw: Microwave treatment at 1 kW.
Th: Thermal treatment at 300 °C or 600 °C.
Ph: Photolytic treatment using solar radiation simulation. Sample was washed in water after photolosis.
(Mw+Th)-A+B: Combined microwave irradiation at 1 kW and thermal treatment at 600 °C for a prescribed length of time (3 or 5 min in the present experiments). No further thermal treatment needed before catalyst reduction at 550 °C.
(Mw+Us)-A: Combined microwave (1 kW) and ultrasound (0.4 kW) treatment.
A: Stage-1a: Catalyst/support precursor fluid formed a porous material followed by decomposition to catalyst oxide after microwave irradiation.

V: Stage-1b: Catalyst/support precursor fluid treated at 300 °C. Temperature of the fluid was raised to 300 °C at a rate of 10 °C/min. After reaching 300 °C, it was kept at this temperature for 30 min before the heating was switched off. After 60 min., the sample was removed and cooled at room temperature (Method-A, Section 3.8)

W: Stage-1c: Catalyst/support precursor fluid was placed in a preheated furnace at 600 °C. After 60 min., the sample was removed and cooled at room temperature. (Method-B, Section 3.8)

X: Stage 1-d: Catalyst precursor fluid was placed in a furnace at room temperature. Temperature was raised to 600 °C at a rate of 10 °C. After reaching 600 °C, the sample was kept at this temperature for another hour. Afterwards, the heating was switched off and the sample cooled down over a period of 24 h (Method-C, Section 3.8).

Y: Stage-1e: Catalyst precursor fluid did not decompose at Stage-1a but formed a porous solid.

B: Stage-2: Catalyst oxide sample from Stage-1a, or Stage-1e was heat treated at 600 °C. Sample temperature was increased at a rate of 10 °C/min from room temperature. After reaching 600 °C, the sample was kept at this temperature for 1 h followed by slow cooling in the furnace over a period of 24 h.

C: Stage-3: Catalyst oxide sample from Stage-1b,c,d or Stage-2 was reduced in hydrogen at 550 °C for 24 h.

D: Stage-4: Reduced catalyst from Stage-3 is used in a reaction.

Therefore, a catalyst sample described as Ni/Si = 1/4 Mw-ABCD means that the catalyst (Ni) and support (SiO_2) molar ratio was 1/4. Catalyst/support precursor fluid was microwaved at 1 kW. It formed a NiO which was then heat treated using the Method-C (Section 3.8) for 2 h followed by slow cooling in the furnace for 24 h. The resulting catalyst oxide was then reduced at 550 °C and used in a reaction.

3.1. Rheological Characteristics of the Catalyst Support Precursor Dispersion

The rheological characterization of the catalyst support precursor dispersion in water was studied using the oscillating pendant drop technique [23] before dissolving the catalyst precursor nitrate salt in the dispersion. The precursor support dispersion, despite its high silica loading, is a clear transparent liquid with relatively low constant simple shear viscosity (10 cp) due to the coating of the dispersed silica particles which reduces silica network formation [27]. In this method, a drop of fluid is generated at the tip of a syringe and the volume of the bubble is oscillated while imaging the bubble. It is important to note that in order to record the image of the oscillating bubble, the pendant bubble is illuminated. It was observed that although a bubble could be generated, during data acquisition, it become unstable and hence the data is confined to the first minute of bubble generation. From this data, the interfacial tension, elastic (storage) modulus (E′) and viscous (loss) modulus (E″) are evaluated as a function of frequency of oscillations using well established theories [23]. The oscillatory variation of the fluid volume and the computed interfacial tension is shown in Figure 1. This data shows that the interfacial tension is unstable, indicating rapid alterations at the air-water interface.

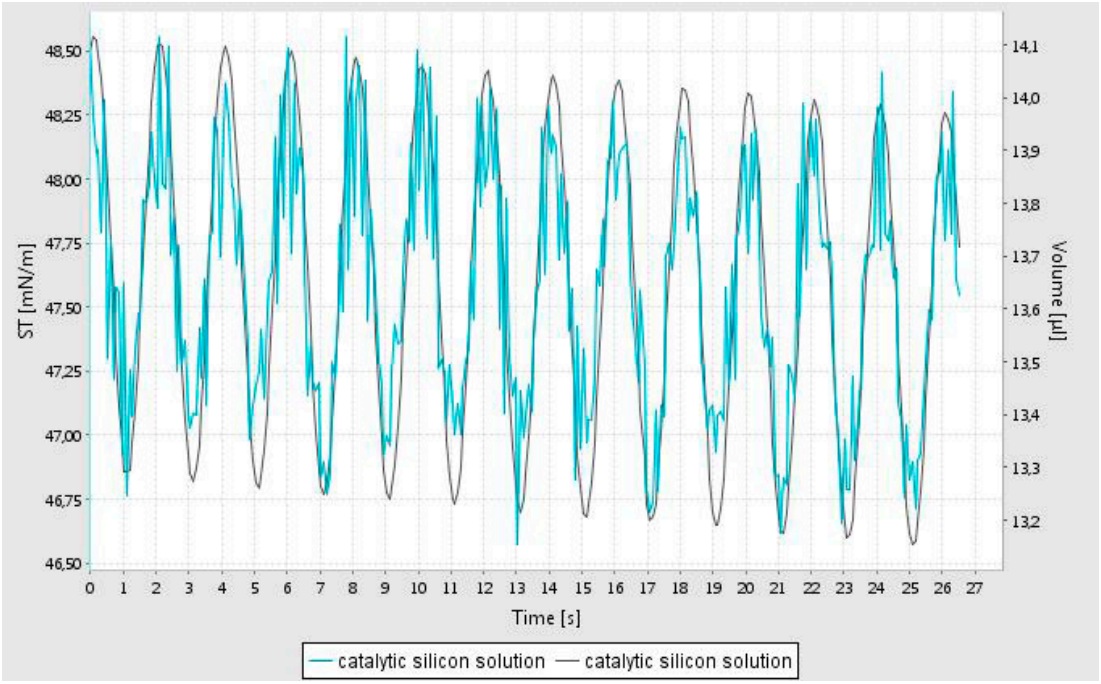

Figure 1. Variation of pendant drop volume (smooth curve) and the computed surface tension (irregular curve) of the silica support precursor dispersion (Bindzil CC30) as a function of time for the measurement of surface rheology.

Although the simple shear viscosity of the dispersion is constant (independent of shear rate in a simple shear flow) it however shows very high fluid elasticity as measured by the oscillating pendant drop method. This non-Newtonian rheological behavior indicates that it has a very high extensional viscosity [27,28] as indeed expected in liquids which are primarily used for surface coating applications. Elastic and viscous moduli (E′ and E″) of the catalyst support dispersion solution were measured at 3 different frequencies (0.2; 0.5; and 1 Hz) and were found to be constant at E′ = 24 $\pm$ 1 mN/m and E″ = 2.3 $\pm$ 0.1 mN/m.

In fact, this behavior has been predicted through the analysis of micro-rheological models of dispersions at oil-water or water-air interfaces using either nearly solid spherical nano-particles [29] or 2-dimensional rod-like particles [30].

When the interfacial rheology of the fluid containing the catalyst precursor nitrate salt (in this case ferric nitrate) and the silica support precursor dispersion was tested, the bubble instability was very fast and the bubble shape could not be fitted for analysis. In any case, instead of forming a bubble, the liquid climbed up the syringe thus no data could be acquired.

The above observations indicate that the fluid surface at air interface has solid-like behavior and that this behavior becomes unstable in the presence of a primary chromophore (nitrate) [31] when the droplet is illuminated, thus producing NO_x and reactive hydroxyl radicals [31] which, in the presence of organic species, (present as silica coating) causes the oxidation of the organic species, as indeed detected by XRD studies (Section 3.12). Furthermore, due to the high storage modulus of the fluid, it is likely that such a fluid is capable of forming thin films despite the fact that it has a very large loading of nano-sized silica particles which can also promote the stability of emulsions/foams [32,33] as well as act as an anti-foaming agent/destabilizer [34] depending on the hydrophobic-hydrophilic balance on the silica surface [32,33].

When ferric nitrate was added to the support precursor silica dispersion, the response of the pendant drop became unstable. It is well known that the orientation or phase behavior of light sensitive molecules (surfactants or surface active moieties) or nano-particles at interfaces can be altered

by using light [35,36]. As nitrate acts as a primary chromophore, which in the presence of organic moieties produces nitrite [31]. This ion is a possible source of NO and hydroxyl radicals [31]. In the case of iron oxide [37] and iron hydroxide [38], we can expect further photocatalytic activity at the air/fluid interface.

These observations formed the bases of modelling of the current technique for the supported catalyst production through self-assembly of the catalyst precursor and silica support.

3.2. TGA Analysis

The results from the thermogravimetric analyzer are shown in Figure 2 which indicates the rapid water loss from silica dispersion while the weight loss from cobalt nitrate solution is the slowest, although at about 220 °C, the rate of weight loss is fastest which corresponds to the decomposition of $Co(NO_3)_2$. In the case of silica containing $Co(NO_3)_2$ solutions ([Co]/[Si] = 1, 1/2; 1/4; 1/9) there are several weight loss steps indicating the formation distinct hydrates and structures. Furthermore, at low temperatures (<50 °C) the weight loss is faster than silica dispersion ([Co]/[Si] = 0).

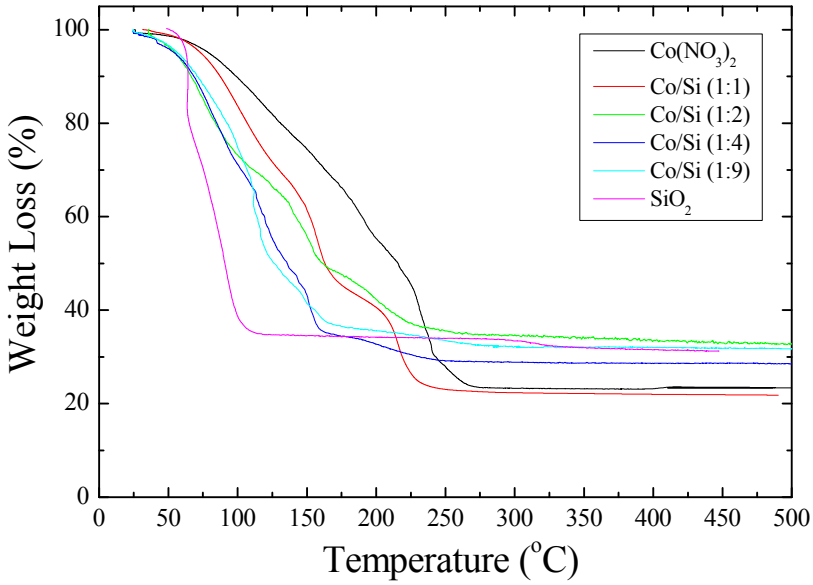

Figure 2. Thermogravimetric analysis of silica dispersion and 1 M cobalt nitrate solution with or without the catalyst precursor solution.

3.3. Pyrolysis of Cobalt Nitrate Solutions

The main decomposition product of cobalt nitrate (as well as that of nickel, iron nitrates) is NO_2 with N_2O and nitric oxide, NO, being the other products [31,39–42]. Here we are not concerned with the detail of the catalyst precursor decomposition but to reveal the effect of coated silica on decomposition. The variation of concentration of NO with temperature during the pyrolysis of cobalt nitrate is shown in Figure 3. It can be seen from this figure that, in the presence of silica ([Co]/[Si] = 1/4), there is a surge of NO even at low temperatures (*ca.* 90 °C) whereas when [Si] = 0, nitric oxide evolution is detected at *ca.* 200 °C. This is in line with the recently published results [41] that the decomposition of d-metal nitrates, NO_2 evolution in the presence of alumina starts at lower temperatures. Furthermore, although the cobalt nitrate concentrations in both samples are the same, the amount of NO evolved in the presence of silica is far in excess of pure cobalt nitrate. In line with the TGA results, Figure 3 also indicates that there are several temperature dependent phases, especially in the presence of silica which alters the kinetics of the decomposition.

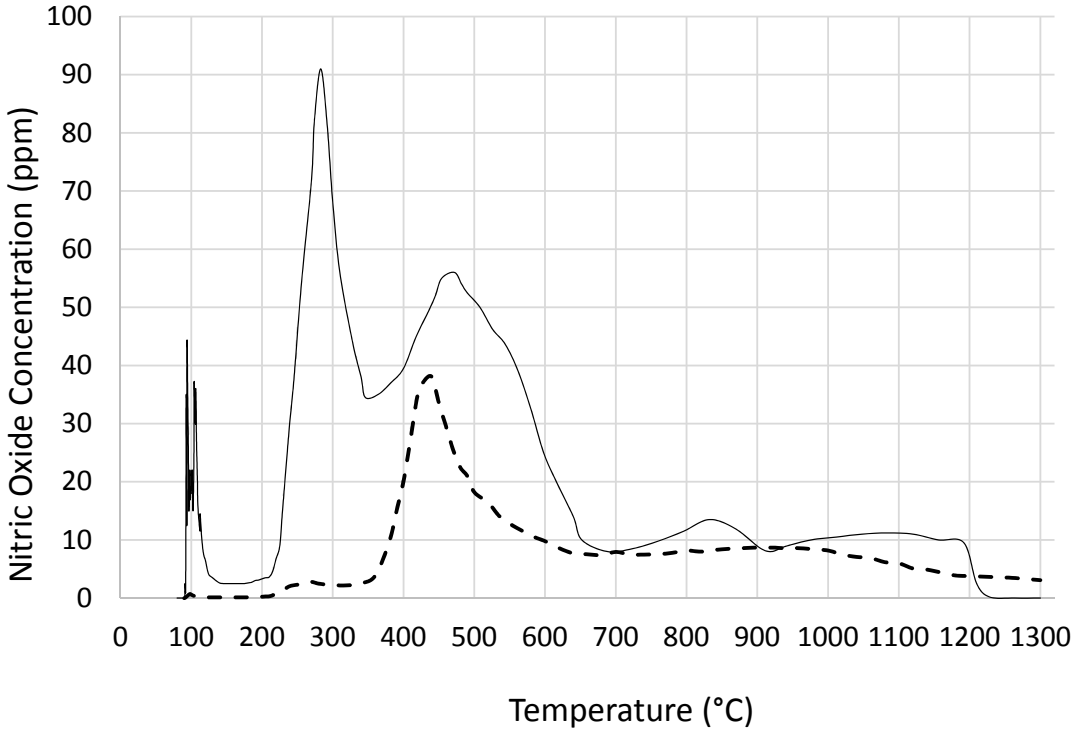

Figure 3. Temperature programmed pyrolysis of cobalt nitrate when: - - - [Si] = 0 and – [Si]/[Co] = 4. Variation of nitric oxide concentration (ppm) with temperature.

3.4. Preparation of Silica Supported Cobalt Catalyst Using the Haake Rheometer

Haake Rheocord Rheometer 9000 was fitted with an internal mixer (Rheomix) with a capacity of 50 mL. This mixer had a reflux condenser to allow vapor to escape and condense outside the mixer during the mixing. It was also used to remove the evolved gases (NO_x). Further details of the Haake Rheometer and Rheomix in this type of operation is available [22]. Two types of experiments were carried out; either using uncoated silica particles or coated silica dispersion (Bindzil CC30) in both cases the size of silica particles were identical at 7 nm.

3.4.1. Uncoated Silica

100 mL of 1 M cobalt nitrate solution was added sufficient amount of uncoated colloidal silica particles (Aerosil AE 380) so as to obtain a paste so that the molar ratio of cobalt and silica is [Co]/[Si] = 1/5. Approximately 50 g of this paste was placed into the Haake mixer while mixing at 60 rpm at room temperature. The mixer temperature was increased to 120 °C. Mixing was continued for 20 min while evaporating water. As the level of material dropped due to the evaporation of water, more of the stock dispersion was added. The resulting paste-like material was recovered and then calcined at 600 °C. The initial furnace temperature was *ca.* 20 °C. The heating rate was 10 °C/min. After reaching 600 °C, calcination was continued for another hour at this temperature before switching off heating to allow the furnace to cool down over a period of 24 h. Afterwards, the sample was recovered for surface area and X-ray diffraction analysis from which the size of the catalyst crystallites could be evaluated. The surface area was found to be 218 m^2/g while the crystal size based on the strongest peak was 23.3 nm.

3.4.2. Coated Silica

In the case of silane coated silica with epoxide functionality, silica dispersion (containing 30 wt % silica) into which a sufficient amount of cobalt or nickel nitrate was added to obtain nitrate solutions

with dispersed silica. This solution is referred to as 'precursor fluid' in which the molar ratio was [Ni]/[Si] = [Co]/[Si] = 1/5. The same mixer as above was used under the same processing conditions in which 50 g precursor fluid was initially used. As the evaporation proceeded, more of the stock solution was added over a period of 15 min. After 20 min of mixing, mixer torque started to increase and a highly viscous paste was obtained. If the mixing continued further, there was a sudden increase in the mixer torque as well as the temperature. These increases were accompanied by a sudden burst of gas evolution (NO_x). After the cessation of gas evolution, the experiment was stopped and the mixer was opened. It was observed that the bulk of the material was still pink (*i.e.*, color of $Co(NO_3)_3$) or green (*i.e.*, color of $Ni(NO_3)_2$) except where the shearing took place on the surface of the mixer wall where it was black, indicating that the decomposition of metal nitrate and the formation of cobalt oxide (CoO and Co_2O_3) or NiO, which were later confirmed by XRD-analysis. The history of mixing of coated silica support and catalyst precursor solution is shown in Figure 4. Samples recovered from the surface and the bulk of the mixture (in the form of paste) were stored for heat treatment to obtain silica supported cobalt or nickel oxide for characterization by SEM, TEM, XRD and BET surface area analysis.

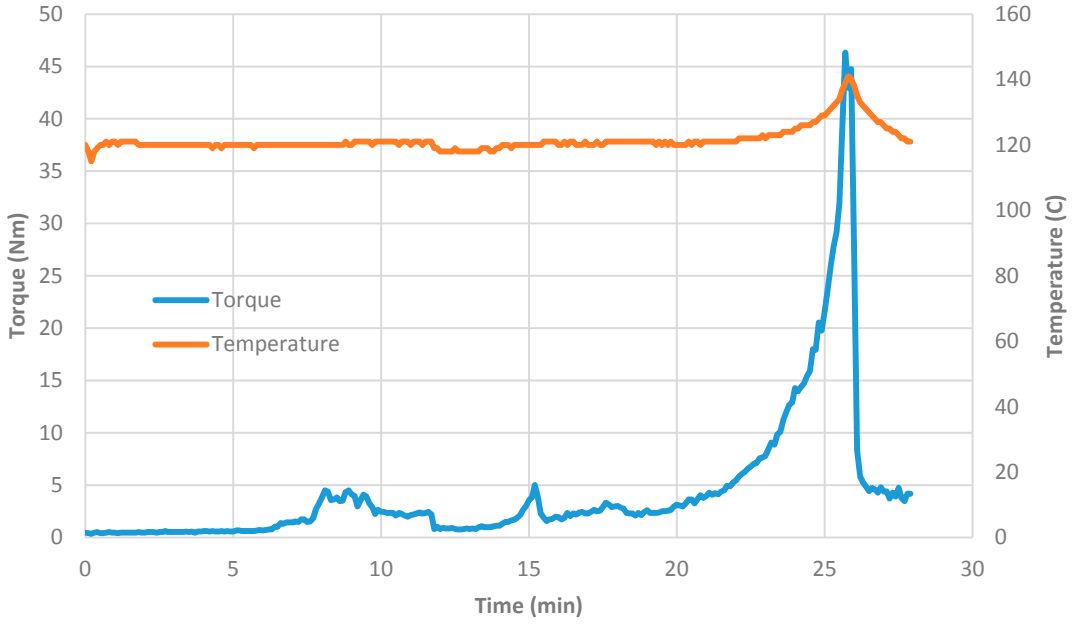

Figure 4. Mixing history of catalyst precursor solution in silica dispersion when [Ni]/[Si] = 1/5.

3.5. Preparation of Coated Silica Supported Catalyst Using GAP-Agglomerator

Supported metal catalysts are often used in agglomerated form. Here, we use a purpose built agglomerator in which liquid feed is converted into agglomerated solid particles after going through a liquid-to-solid phase transformation. This technique is known as flow induced agglomeration originally developed for polymeric systems [43,44]. The agglomerator consists of a rotor and stator which have closely packed cavities. These cavities can pump, convey highly viscous phases and after phase inversion, also convey the newly formed particles. The diagrammatical illustration of the GAP-agglomerator is shown in Figure 5. The cross-section of the agglomerator (Figure 5a) also illustrates the cooling and heating zones as well as ports for the removal of vapors and gases. The top-view of the agglomerator illustrates (Figure 5b) the location of the vapor/gas removal ports. The cavity shape and their distribution on the rotor are shown in Figure 5c.

The entrance to the rotor/stator of the agglomerator was kept at 90 °C while the rest of the disks were kept at 120 °C. The rotational speed was 30 rpm. Coated silica dispersion containing catalyst precursor, $Co(NO_3)_2$ at a molar ratio of [Co]/[Si] = 1/5 at room temperature was pumped into the equipment at a rate of 10 mL/min. Vapor was allowed to escape from the vapor ports as well as from

the gap between the disks at the outlet. Catalyst precursor/support dispersion went through a highly viscous phase as the water content decreased. The constant mixing, and the design of the agglomerator cavities allow pumping of the highly viscous dispersions which eventually 'crumbles' and primary particles agglomerate. Agglomerated particles were discharged at the exit between the disks and were collected in the collection tray.

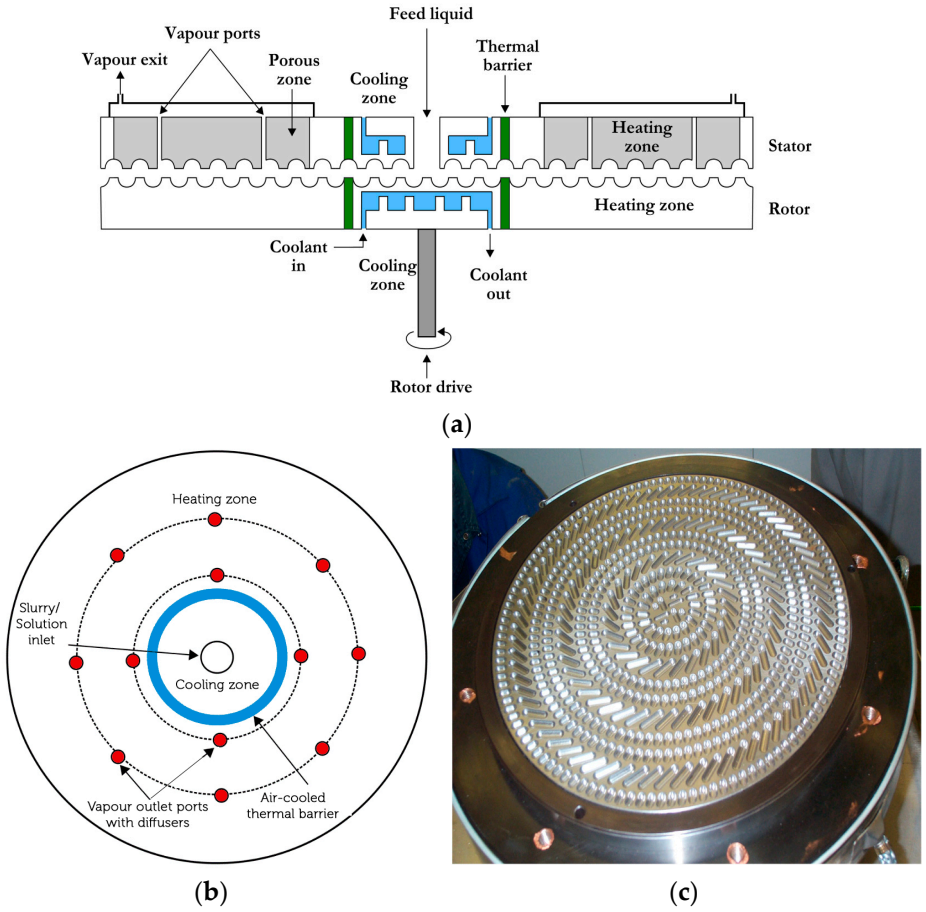

Figure 5. Equipment for the production of agglomerated dense catalysts. (**a**) Cross-section of the rotor-stator system with different functional regions; (**b**) Top view of the equipment illustrating location of various inlets and outlets; (**c**) Photograph of the rotor showing the cavity shape and distribution.

The particle size measurements indicate that the average particle size of the agglomerates was D_{50} = 155 µm; particle size at 10% and 90% cumulative were D_{10} = 42 µm and D_{90} = 320 µm respective while the particle size span was S = 1.08 indicating a very narrow size distribution. These samples were calcined as described in Section 3.1. The resulting supported metal oxide was analyzed for surface area and catalyst size from XRD. Supported catalyst surface area was 238 m^2/g while the cobalt oxide size based on the strongest XRD-peak was 21.1 nm.

3.6. Supported Catalyst Generation within the Pores of Macro-Porous Foams

In chemical reactors, catalysts are used in a fixed bed or fluidized bed. Alternatively, catalysts can be fixed on the walls of so called structured or monolithic or micro-reactors. However, in such reactors, catalyst fixation on the reactor walls has some drawbacks, including low catalyst volume and a tendency for catalyst to erode, due to fluid flow and thermal/mechanical stress generation.

In order to prevent these drawbacks, the catalyst can be incorporated within the pores of metallic or ceramic foams which can then be fabricated into micro-reactors as illustrated in Figure 6.

Microreactor fabrication (such as micro-capillary reactors) using metallic foams containing catalysts is especially simple since a series of parallel half capillaries or other types of channels can be formed and subsequently these plates can be assembled to form micro-channel reactors as shown in Figure 6a. Main bulk flow of the reactants will be in these channels but they will readily diffuse into the foamed regions where the catalyst is present. The flow field can be tailored to promote heat and mass transfer through the geometry/architecture of these foamed structures. For example, the basic flat units with imprinted half capillaries can be off-set so that the channels are capillaric or even fully open in the transverse direction (Figure 6b). Further facilitation in such reactors can be achieved by separating each structured plate by non-porous thin metal plates so that two sets of separate inlets-outlets can be obtained to carry out separate reactions in each set. Such systems are useful for rapid heat transfer.

In such porous channel reactors, catalyst erosion due to stresses generated through fluid flow and/or thermal gradients are prevented since the transport processes (momentum, heat and mass transport) are not by convection but through diffusion and the foam structure allows the absorption of thermal and mechanical stresses.

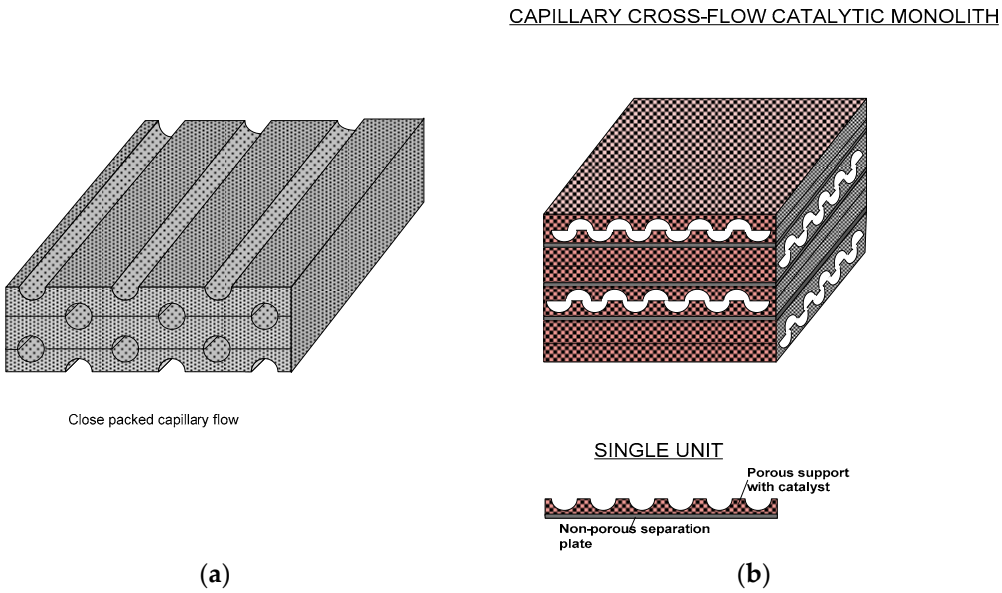

Figure 6. Various micro-capillary reactors formed by macro-porous metal foams filled with supported catalysts.

We used a nickel foam in order to incorporate silica supported cobalt catalysts. This system allows us to distinguish between the foam support (Ni) and the catalyst (Co) in XRD analysis. A support precursor fluid (Bindzil CC30) and cobalt catalyst precursor ($Co(NO_3)_2$) solution was prepared at the molar ratio of [Co]/[Si] = 1:4. Flat nickel foam (Recemat) plates, measuring 10 cm × 10 cm, were pressed against a set of 1 mm diameter stainless steel rods separated by 2 mm spaces in a hot press at 300 °C and 10 bar pressure for 2 min to form an imprint of the rods in the form of half capillaries. These plates were then soaked in the support + catalyst precursor fluid for 10 min and then placed in flat dishes with sufficient support + catalyst precursor solution covering them. These plates were then put into a furnace and heat treated at 600 °C (with 1 h heating time at a rate of 10 °C/min and 1 h dwell time at 600 °C followed by 24 h of cooling). Any excess catalyst from the surface was removed in an air stream and then examined under SEM followed by XRD analysis for the crystallite size of the silica supported cobalt oxide catalyst.

Figure 7 shows the presence of cobalt catalyst within the pores of the nickel foam while Figure 8 illustrate the XRD-pattern of this catalyst system. Very sharp dominant peaks represent nickel while the smaller and broader peaks represent Co_3O_4 with crystallite size of 20.9 nm based on the dominant cobalt oxide peak at $2\theta = 36.6^\circ$.

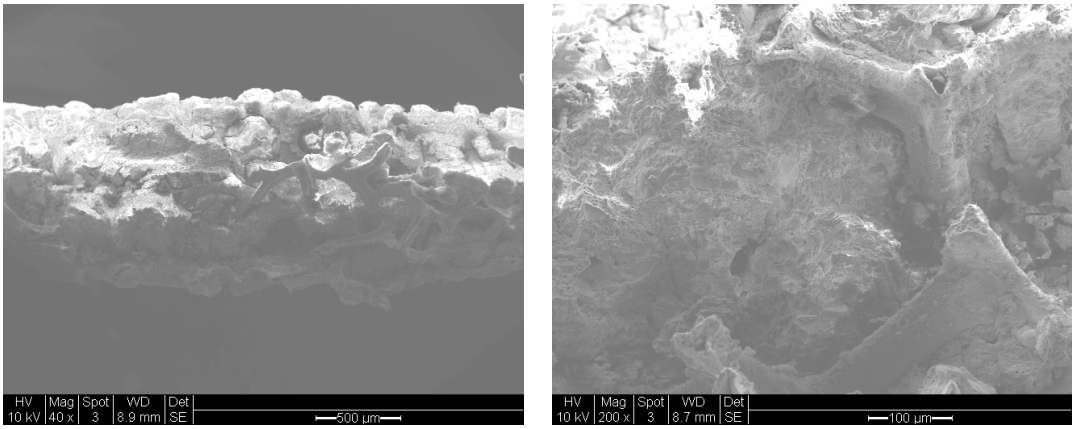

(**a**) (**b**)

Figure 7. Scanning electron microscopy of silica supported cobalt catalyst macro-porous nickel foam. (**a**) Overall appearance of the fracture surface of the foam with catalyst (scale bar = 500 µm); (**b**) At large magnification showing the walls of the nickel foam in a large pore with the porous supported catalyst. (scale bar = 100 µm).

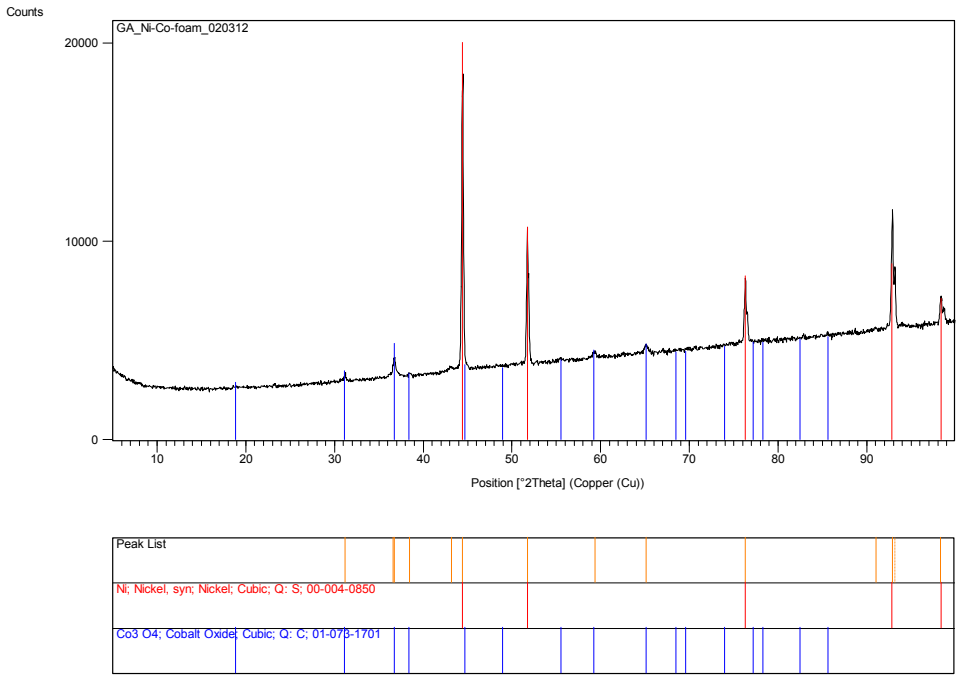

Figure 8. X-ray diffraction pattern of silica supported cobalt catalyst in macro-porous nickel foam.

3.7. Supported Catalyst Generation Using Microwave Radiation

3.7.1. Microwave Radiation with Variable Power

A microwave reactor (Ethos One) supplied by Milesone Srl, Italy, was used in order to evaluate the effect of microwave power on the supported catalyst properties. We used either cobalt nitrate or nickel nitrate as catalyst precursor and Bindzil CC 30 as support precursor. The molar ratio of [Co]/[Si] = [Ni]/[Si] = 1/5. This equipment allows the measurement of temperature during microwave irradiation and microwave radiation power can be controlled. Twenty milliliters of catalyst + support precursor fluid was placed in a 250 mL round bottom flask fitted with a temperature probe. The flask was placed on a rotating stand and the fumes/vapor generated was extracted continuously. As seen in

Figure 9, the temperature of the fluid increases to *ca.* 115 °C where it remains during the evaporation of water. Immediately after the evaporation is complete, the decomposition of the catalyst precursor salt starts with the evolution of NO_x which is completed by the time the temperature reaches 225 °C. The temperature of the sample was not allowed to rise above 225 °C. At this cut-off temperature, microwave radiation was stopped, fumes were allowed to be fully extracted and the sample was removed. Typical time-temperature profiles for cobalt and nickel are shown in Figure 9a,b which indicates that the rate of reaction for Co is faster than that for Ni. At the maximum power input, the reaction is complete within 90 s for cobalt and 120 s for nickel.

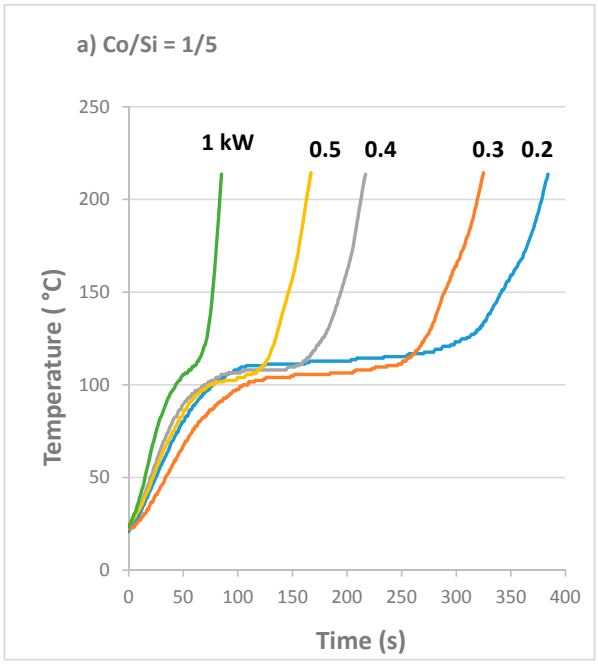

(**a**)

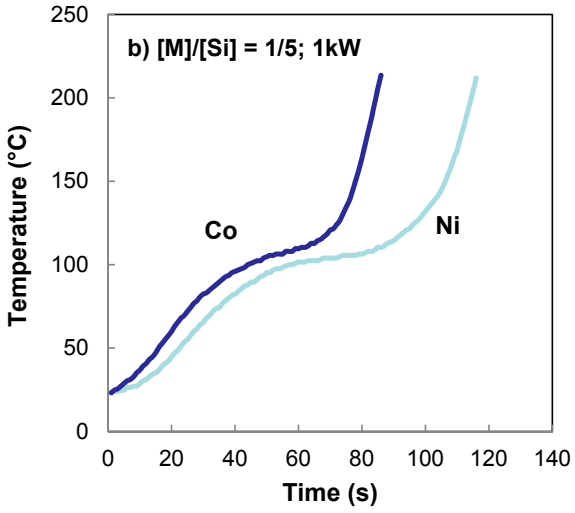

(**b**)

Figure 9. Processing history of silica supported cobalt and nickel catalysts from nitrate solution and coated silica dispersion using microwave radiation at various power ratings when [Co]/[Si] = [Ni]/[Si] = 1/5. (**a**) The effect of microwave power on cobalt nitrate decomposition in the presence of coated silica; (**b**) Comparison of cobalt and nickel on the decomposition rate of nitrate.

During microwave irradiation of catalyst (M) (where M = Fe, Co, or Ni in the current study) precursor fluid starts boiling at *ca.* 115 °C and an expanded/porous solid mass is obtained. This material is in fact still metal nitrate salt as there is no color change in the metal nitrate. If the radiation was continued, provided that the radiation power was sufficient, a rapid decomposition of catalyst nitrate occurred with the evolution of NO_x.

3.7.2. Microwave Irradiation at Constant Power

Microwave irradiation at a constant power of 1 kW was carried out using a Panasonic kitchen microwave oven with a turn-table. We used watch glasses to contain the metal nitrate solution and silica dispersion (precursor fluid). We used 5 mL of the precursor fluid in a 9 cm diameter watch glass or 10 ml solution in a 19 cm watch glass. It was found that if the boiling was suppressed, the volume of the expanded catalyst precursor salt as well as of the decomposition product (metal oxide) were reduced. This is shown in Figure 10 for nickel. In Figure 10a, although the bulk of the material has decomposed to form nickel oxide, at the edge of the reaction zone, where the liquid film anchors to glass, there was no decomposition of nickel nitrate as evident from the light green coloring. In Figure 10b, it can be seen that, due to extensive anchorage, film formation had been suppressed (when the precursor fluid was contained in a Petrie dish) and therefore both the formation of porous material and decomposition were suppressed.

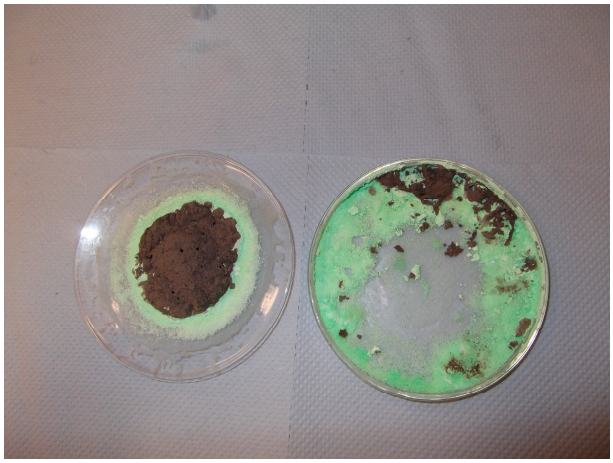

(**a**) (**b**)

Figure 10. The effect of film formation on the structure of the material after the evaporation of water and decomposition of nitrate salt during microwave radiation of 1 M nickel nitrate in coated silica dispersion ([Ni]/[Si] = 1/4. (**a**) Reaction in a watch glass; (**b**) Treatment in a Petrie dish. Black regions contain NiO while the green regions are nickel nitrate.

The nitrate decomposition reaction starts from the center of the expanded supported nitrate salt and spreads radially downwards. Although the reaction is rapid (typically 30 s), the reaction stops, if the microwave is stopped.

It was found that for a given concentration ratio of catalyst (M) and support (Si) [M]/[Si] (where M = Fe, Co or Ni) there was a threshold power below which the decomposition reaction did not take place and black metal oxide did not form although the solution formed an expanded porous structure. This critical microwave power (P^*) is dependent on the source of the catalyst, pH of solution as well as the [M]/[Si] ratio. P^* decreases with decreasing [M]/[Si] ratio. For Co and Ni at natural pH of the solution (pH = 5.5) decomposition of the catalyst salt did not take place at P^* = 1 kW when [M]/[Si] $\geqslant$ 0.5. Under these conditions thermal treatment at 600 °C was used to obtain the supported catalyst oxide. However, we have not systematically investigated the variation of P^* with the chemical composition of the precursor fluid.

3.8. Thermochemical Preparation of Supported Catalysts

In order to use the supported metal oxide obtained from the catalyst precursor nitrate salt, it is necessary to reduce the resulting metal oxide for use as a catalyst. Furthermore, the organic coating on the catalyst support needs to be removed, unless it has a catalytic functionality. This coating can also be carbonized to obtain a mixed silica/carbon catalyst support.

The catalyst oxide reduction can be carried out typically at 550 °C using hydrogen. The type of catalyst developed here is also suitable as a high temperature heterogeneous catalyst and has been used in gas-to-liquid conversion processes [45–47] including dry reforming [45], ammonia synthesis [46] and Fischer-Tropsch synthesis [47]. However, high temperature catalyst oxide reduction or high temperature catalytic processes result in the enlargement of the catalyst size. Therefore, the catalyst oxide size after thermal treatment at high temperature will be a more realistic characteristic of the catalysts. Nevertheless, it is also possible to use these catalysts successfully for low temperature gas-to-liquid conversion processes using non-thermal plasma when the catalyst reduction is carried out in-situ at low temperatures, <250 °C [8,45–47].

It was also found that if the molar ratio of catalyst and support, [*M*]/[Si] (where *M* = Fe, Co, Ni in present case) is large or the pH is too low, the nitrate decomposition reaction did not take place although the highly porous (expanded) catalyst/silica precursor structure was formed.

For the reasons listed above, we also carried out the decomposition reaction of catalyst nitrate/silica support at 300 °C or 600 °C. Experiments at 300 °C were carried out in order to directly compare the thermal process with the microwave process although the maximum temperature in the microwave process was 225 °C and the decomposition reaction actually started at *ca.* 125 °C.

It was found that the thermal preparation of the catalyst using coated silica at 300 °C and 600 °C also resulted in film boiling and subsequent decomposition of nitrate to catalyst oxide and the formation of a highly porous catalyst. As described previously (Sections 3.2 and 3.3) we have already prepared catalysts at 600 °C when the supported catalyst precursor underwent decomposition from a highly viscous state, without forming a film. Therefore, the comparison of catalysts obtained from these two methods should illustrate the mechanism of catalyst structure formation using microwave radiation.

We used the following methods for the thermal processes:

(a) Thermal decomposition with boiling at 300 °C (Method-A): 20 mL of the precursor solution containing Bindzil CC 30 and nickel nitrate was placed in a 1 liter beaker and placed in a high temperature furnace. The temperature was raised from room temperature to 300 °C at a rate of 10 °C/min. The sample was kept at this temperature for another 30 min before the heating was switched off. After a period of *ca.* 0.1 h, the sample was recovered in the form of an expanded black solid and subsequently analyzed for surface area, crystallite size and micro-to-nano size structure evaluation.

(b) Thermal decomposition with boiling at 600 °C with rapid heating-rapid cooling (Method-B): 20 mL of the precursor solution containing Bindzil CC 30 and nickel nitrate was placed in a 1 liter beaker and placed in a high temperature furnace. Temperature of the furnace was raised to 600 °C and the sample was put into the furnace. After a period of 0.1 h, the sample was removed and allowed to cool at room temperature.

(c) Thermal decomposition with boiling at 600 °C with slow heating-slow cooling (Method-C): After placing the precursor solution sample into the furnace, its temperature was raised from room temperature to 600 °C at a rate of 10 °C/min. The sample was kept at this temperature for another 60 min before the heating was switched off. After a period of 24 h (slow cooling process), the sample was recovered in the form of expanded supported metal oxide and subsequently analyzed for surface area, crystallite size and micro-to-nano size structure evaluation.

Method-C was also used to calcine the samples from microwave treatment, either as expanded silica supported metal nitrate (*i.e.*, decomposition has not taken place) or as silica supported metal oxide (after decomposition of the nitrate salt) in order to compare the two methods.

3.9. Combined Thermal and Microwave Processing

A Milestone microwave reactor (Pyro XL) was used for the microwave irradiation of the support dispersion and catalyst (nickel nitrate) precursor fluid at 600 °C. 5 mL solution was placed in ceramic crucibles and inserted into the preheated high temperature microwave reactor and the microwave radiation started. The radiation continued either for 120 s or 300 s, at the end of which the samples were removed immediately and allowed to cool at room temperature. Samples were then analyzed for surface area, XRD, SEM and TEM for comparison with the thermal or microwave only methods.

3.10. UV-Radiation Induced Decomposition of Catalyst Precursor in Silica Dispersion

It was observed that ferric nitrate solutions in the presence of coated silica dispersion ([Fe]/[Si] $\leqslant$ 1/3) was unstable when exposed to solar radiation and produced NO_2 while the solution gradually solidified with expansion. Photo-sensitivity of $Fe(NO_3)_3$ in the presence of coated silica was further confirmed during the "Pendant Drop" tests as described previously. The molar ratio of the catalyst to support was [Fe]/[Si] = 1/4 or 1/3. Under solar radiation, the precursor fluid appeared to bubble and flakes of mixed silica and iron oxides raised over the liquid, similar to the foam extraction process. In the meantime, the liquid became highly viscous.

In order to replicate these experiments, an agricultural plant growth cabinet which simulates solar radiation and atmospheric conditions (such as temperature and humidity) was used for the model solar irradiation. The growth cabinet operated continuously and in order to prevent the rapid evaporation of water from the solution, the relative humidity was kept at 50% while the temperature was constant at 25 °C. We used two types of dishes to contain the catalyst/support precursor fluid.

Method 1: Round bottom 9 cm diameter watch glasses to which was added 5 mL of the catalyst/support precursor fluid.

Method 2: 50 mL capacity glass beakers to which was added 10 mL catalyst/support precursor fluid.

These fluids were place on the sample tray of the agricultural growth cabinet and the solar simulant radiation was started. The radiation level of the growth cabinet was set at the maximum, giving a radiation dose at LUX = 82,000 lx. Radiation was continued for up to 120 h continuously.

It was found that when the round bottom watch glasses were used, a dense but porous mixed oxide was obtained. However, when $Fe(NO_3)_3$ with silica dispersion was used by itself in the glass beaker, iron oxide flakes started to form and travelled to the top of the beaker where they accumulated or fell over the side towards the end of the irradiation. These observations are illustrated in Figure 11. As seen in Figure 11a, when [Fe]/[Si] > 1/3 the decomposition of ferric nitrate does not take place. When [Fe]/[Si] $\leqslant$ 1/3 and a glass beaker was used, flakes of iron oxide traveled upward as flakes, while in a watch glass, formed flakes fell back into the solution.

(**a**) (**b**)

Figure 11. Photo-irradiated $Fe(NO_3)_3$ in silica dispersion after 70 h in a beaker or in a watch glass. (**a**) In a beaker when [Fe]/[Si] = 1/3 (No. 13); 1/2 (No. 12) and 1/1 (No.11); (**b**) In a watch glass when [Fe]/[Si] = 1/3.

Several other metal nitrates with coated silica ([*M*]/[Si] = 1/4) were also tested, including Al, Mg, Ca, Co, Ni, Zn and Mn. None of these metal nitrates decomposed even after 60 days of UV irradiation in the growth cabinet. However, Co solution ([Co]/[Si] = 1/4) appeared to form a gel on the surface which however disappeared after the removal of UV-radiation.

The XRD analysis of these decomposition samples ([Fe]/[Si] = 1/4 or 1/3) showed the formation of Fe_3O_4 (magnetite). They were then heat treated at 600 °C (1 h heating time and 1 h dwell time followed by 24 h of cooling). Samples which were not heat treated after UV-irradiation were washed in water to remove any unreacted nitrate, and then they were subjected to XRD, BET, SEM and TEM analysis.

3.11. Reduction of Supported Catalysts

In some cases, after full evaluation of the catalyst characteristics based on the catalyst oxide, some of the catalysts were reduced and used in various applications. The cobalt catalyst was used in Fischer-Tropsch synthesis [47] and the nickel catalyst was used in ammonia synthesis [46] and dry reforming [45]. Reduction was carried out at 550 °C using H_2 at atmospheric pressure. Details of the reaction and method of reduction are available [8]. The purpose of the catalyst reduction was to test the performance of these catalysts in various reactions. One of the advantages of catalyst reduction for catalyst structure evaluation using SEM at high magnifications is that the sample does not need to be coated with a conductive layer.

3.12. Analysis of the XRD and BET Surface Area Results

The purpose of this XRD study is primarily to determine the composition of the supported catalysts at various stages and to determine the size of the catalyst crystallites size using the Scherrer method [24,25]. TEM imaging is often used to determine the catalyst size and its distribution to supplement the data from XRD.

Below we give the basic XRD data for silica supported nickel, cobalt and iron catalysts at various stages of processing in order to establish the mechanism of catalyst structure formation as a function of processing conditions and composition and to evaluate the catalyst size.

3.12.1. Ni/Si Catalyst

Figure 12 represents the XRD pattern of silica supported nickel at various stages of processing. In all cases [Ni]/[Si] = 1/4. The XRD pattern in Figure 12a is that of Ni/Si when the catalyst precursor fluid at pH = 0.2 was irradiated at 1 kW to form an "expanded green material". The surface area of this material was found to be 235 m^2/g. If the irradiation of this precursor fluid were to be carried out at its natural pH (pH = 5.5), the expanded green material would start to decompose immediately after its formation. Therefore, it is also possible to stop the decomposition of the 'expanded green material' when pH = 5.5, by stopping the microwave irradiation. This material was removed and subjected to XRD and BET analysis. The surface area of this "expanded green material" (pH = 5.5) was found to be 208 m^2/g, indicating that the pH does effect the catalyst structure.

In Figure 12a, the dominant band at $2\theta = 22.1^\circ$ represents SiO_2. The second major band at $2\theta = 12.7^\circ$ or the peak at $2\theta = 59.6^\circ$ were not identified whereas the bands at 11.1° and 25.5° were identified as nickel nitrate hydroxide hydrate [$Ni_2(NO_3)_2\ (OH)_2 \cdot 2H_2O$] and the bands at $2\theta = 30.3^\circ$ were identified as nickel oxalate dehydrate, $NiC_2O_4 \cdot 2H_2O$ which decomposes to yield NiO. The formation of nickel nitrate hydroxide hydrate reflects the fact that the initial reaction takes place in solution at relatively high temperatures and that the formation of nickel oxalate hydrate can be considered to be due to the epoxide functional silane coating present on the silica particles. In the absence of any knowledge about the unidentified bands, the nature of the reactions during the transformation from catalyst precursor fluid to solid state cannot be concluded.

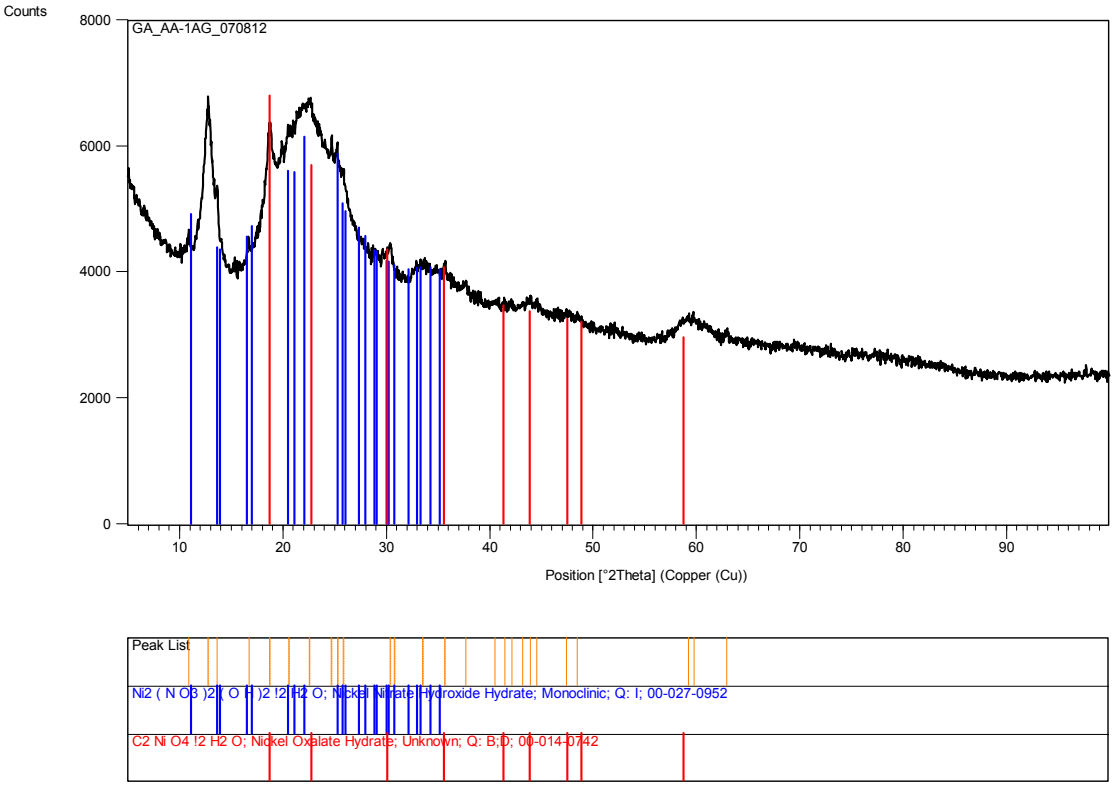

(**a**)

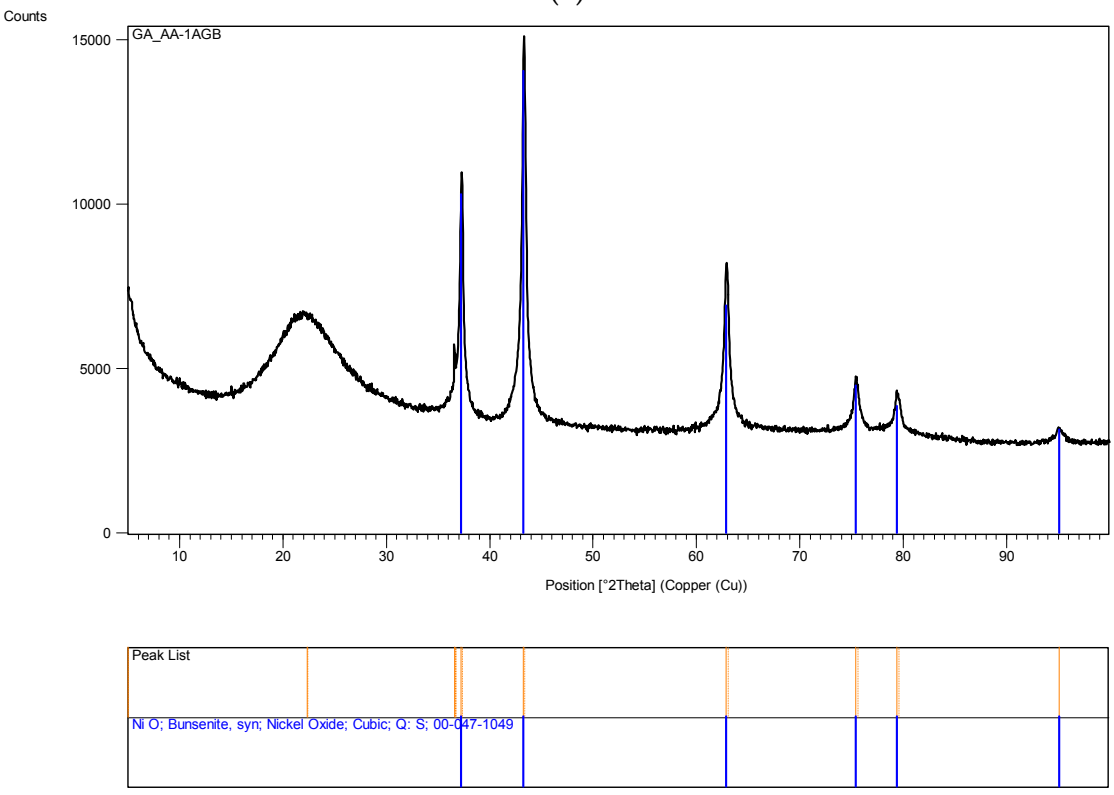

(**b**)

Figure 12. *Cont.*

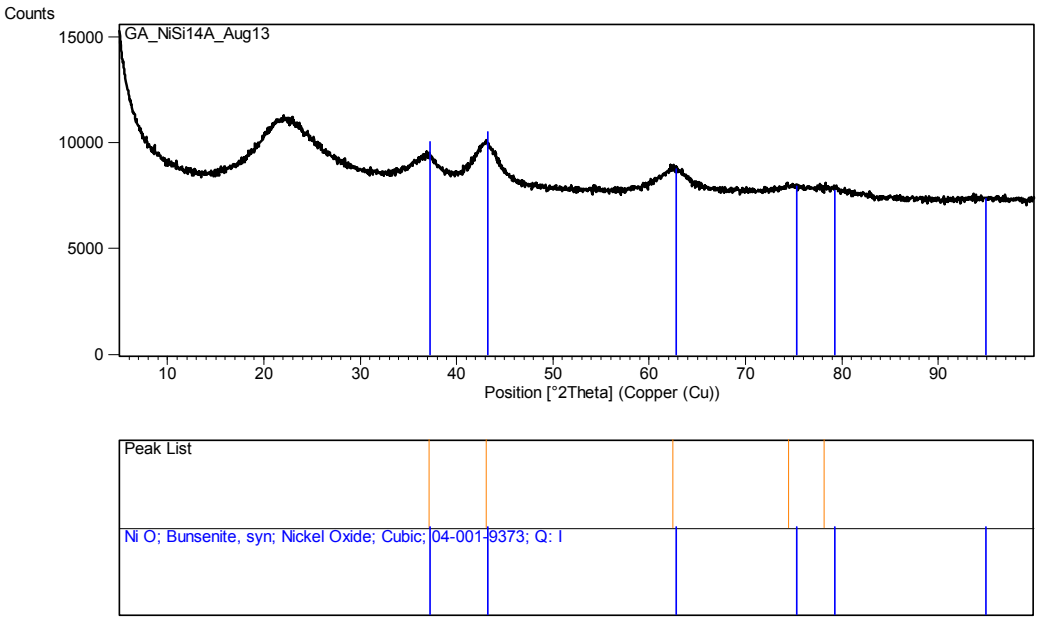

(**c**)

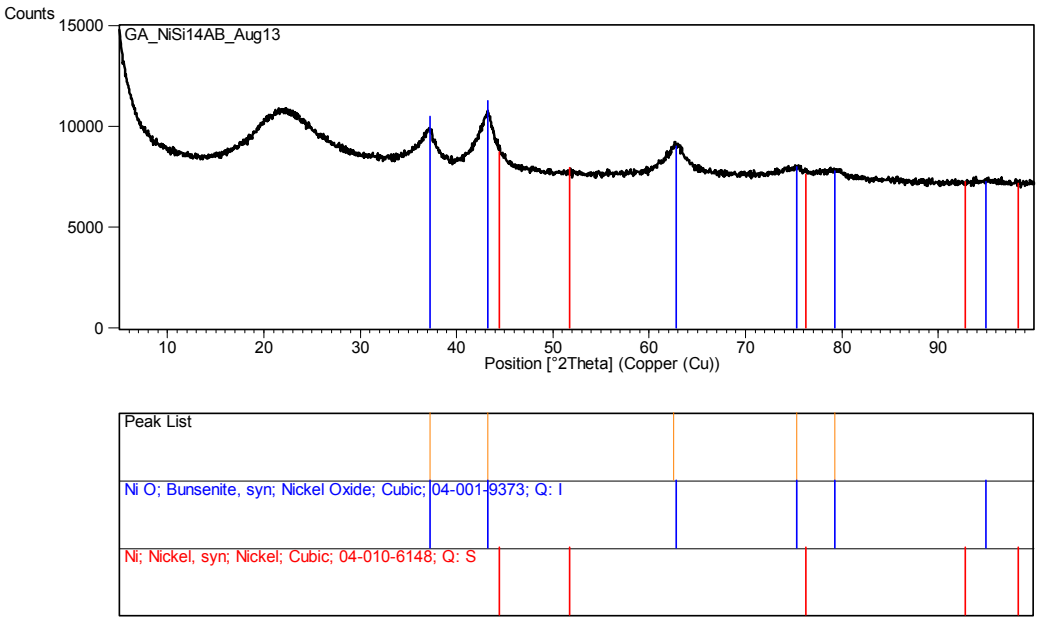

(**d**)

Figure 12. *Cont*.

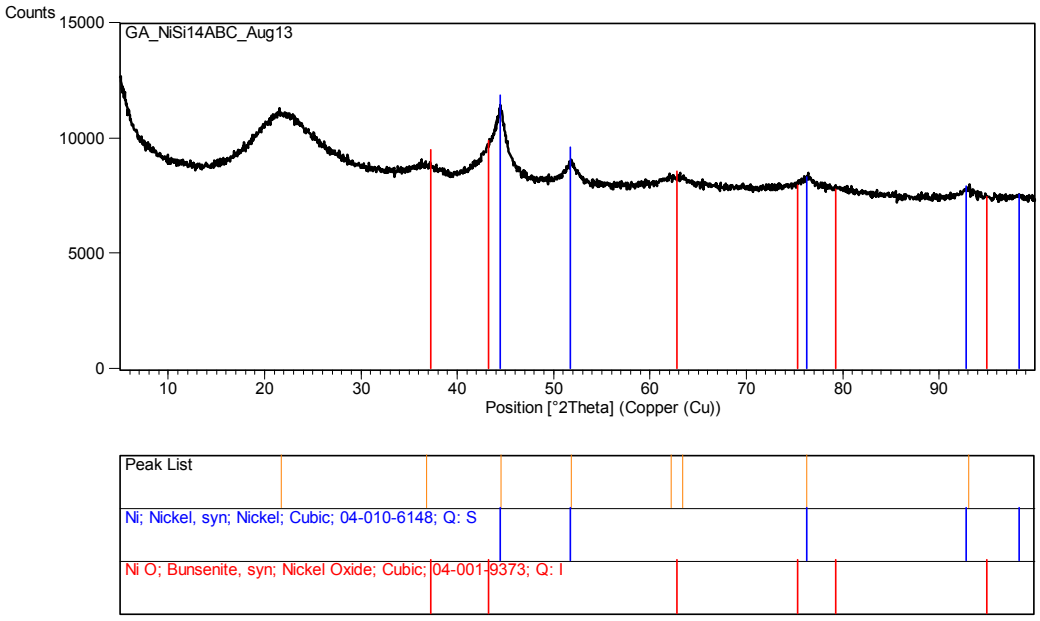

(**e**)

Figure 12. (**a**) XRD pattern of the sample Ni/Si = 1/4 Mw-Y pH = 0.2: Nickel nitrate silica precursor fluid ([Ni]/[Si] = 1/4) microwaved at 1 kW but it was not fully decomposed because pH = 0.2. An alternative method is to stop the microwave radiation immediately after the start of decomposition and remove the green and black parts separately; (**b**) XRD pattern of the sample in Figure 12a [Coded as Ni/Si = 1/4 Mw-YB pH = 0.2] after its heat treatment at 600 °C (1 h heating and 1 h dwell time followed by 24 h cooling in the furnace); (**c**) XRD pattern of the catalyst precursor dispersion/solution (Sample Ni/Si = 1/4 Mw-A; pH = 5.5) after it was microwaved at 1 kW forming a black supported nickel oxide; (**d**) XRD pattern of the sample Ni/Si = 1/4 Mw-AB from Figure 12c when the microwave irradiated catalyst precursor dispersion/solution at pH = 5.5 was subjected to heat treatment at 600 °C; (**e**) XRD pattern of silica supported nickel catalyst (Ni/Si = 1/4 Mw-ABC) after the reduction process by hydrogen using the sample in Figure 12d.

The above samples were subsequently calcined at 600 °C. Starting from room temperature, the sample was heated in a furnace at a rate of 10 °C/min. The sample was kept at this temperature for 1 h and then the heating was stopped, allowing the furnace to cool down over 24 h before removing the sample. The surface area of the calcined sample, (Ni/Si = 1/4 Mw-YB; pH = 0.2), was 203 m^2/g being reduced from 235 m^2/g. The same heat treatment of the "expanded green material" obtained at pH = 5.5 (with surface area of 208 m^2/g) resulted in a surface area reduction to 196 m^2/g when it was calcined under the same conditions (sample Ni/Si = 1/4 Mw-YB; pH = 5.5).

The XRD pattern of this sample (Ni/Si = 1/4 Mw-YB; pH = 0.2) obtained from the heat treatment of Ni/Si = 1/4 Mw-Y at 600 °C) is shown in Figure 12b. It can be seen that in addition to the very broad silica peak at 2θ = 21.9°, there are only NiO peaks at 2θ = 36.9°; 43.2° (dominant peak); 62.7° and Ni peaks at 31.2°; 44.5° (dominant peak); and 51.9° are absent. The catalyst size before reduction (NiO) and after reduction (Ni) were calculated from the Scherrer equation using the dominant peaks at 2θ = 43.2° and 44.5° respectively. The crystallite size of the sample (Ni/Si = 1/4 Mw-YB; pH = 0.2) was found to be 43.3 nm whereas the crystallite size of the sample (Ni/Si = 1/4 Mw-AB; pH = 5.5) processed at pH = 5.5 was only 4.49 nm. Note that these diffraction angles can change slightly from sample to sample depending on the processing conditions.

If the catalyst precursor fluid ([Ni]/[Si] = 1/4) at its natural pH (= 5.5) was microwaved at 1 kW for 3 min, initially, the 'expanded green material' was formed and further irradiation resulted in the formation of 'black' nickel oxide within 45 s. The XRD pattern of this material is shown in Figure 12c

which indicates that the primary product is NiO and SiO_2 although some possible contamination is present as nickel oxide hydroxide [$Ni_2O_2 \cdot (OH)_4$]. However, no quantitative evaluation of this compound could be made. It can be seen that the NiO peaks in Figure 12c are broader than those present in Figure 12b. When the material from this microwaved NiO was heat treated as described for the sample in Figure 12b, the resulting XRD pattern shown in Figure 12d, indicates that the NiO peaks also become sharper indicating enlarged catalyst oxide size.

XRD pattern of the silica supported nickel catalyst ([Ni]/[Si] = 1/4 Mw-ABC) is shown in Figure 12e after reduction in the hydrogen atmosphere at 550 °C for 24 h. The catalyst was obtained from the sample described in Figure 12d. Figure 12e indicates that some NiO remained in the catalyst which is due to re-oxidation when the catalyst is exposed to air for XRD-analysis.

It is also possible to obtain non-decomposed nickel/silica solid catalyst precursor from a dispersion/solution at pH = 5.5 in the form of 'expanded green material' by stopping the microwave irradiation just before the decomposition of nitrate starts. After removing NiO from the non-decomposed part, the sample was subjected to XRD and BET analysis. In this case the composition was [Ni]/[Si] = 1/3.

One of the reasons for heat treatment at 600 °C is to burn-off the silane coating on the silica. Therefore, it is also possible to combine the microwave irradiation with thermal treatment at 600 °C. This treatment is suitable for the continuous production of supported catalyst oxide with small (*ca.* 5 min.) residence time. The weight percent of carbon on the nickel oxide/silica (Ni/Si = 1/4) after combined microwave (1 kW) and thermal treatment at 600 °C (Mw+Th) was 0.18% after 120 s and 0.05% after 300 s of microwave and thermal treatment. Table 1 summarizes the above results, including the BET surface area and NiO or Ni size following the above treatments.

Table 1. The effect of pH and processing conditions at various stages on the surface area and catalyst crystallite size based on the dominant XRD peak.

Sample Code	[Ni]/[Si]	pH	NiO Size (nm)	Ni Size (nm)	Surface Area (m^2/g)	Comments
Ni/Si = 1/4 Mw-Y	1/4	0.2	-	-	235	No heat treatment
Ni/Si = 1/4 Mw-YB	1/4	0.2	43.3	-	203	Heat treatment at 600 °C
Ni/Si = 1/4 Mw-A	1/4	5.5	3.50	-	208	No heat treatment
Ni/Si = 1/4 Mw-AB	1/4	5.5	4.49	-	196	Heat treatment at 600 °C
Ni/Si = 1/4 Mw-ABC	1/4	5.5	3.08	2.76	183	Catalyst reduction after heat treatment at 550 °C
Ni/Si = 1/4 Th-X	1/4	5.5	5.65	-	217	Precursor fluid directly heat treated at 600 °C
Ni/Si = 1/3 Mw-AB	1/3	5.5	4.16	-	173	Heat treatment at 600 °C
Ni/Si = 1/3 Mw-YB	1/3	5.5	4.92	-	177	Heat treatment at 600 °C
Ni/Si = 1/4 (Mw+Th)-A+B (3 min)	1/4	5.5	3.81	-	214	Combined microwave & thermal treatment at 600 °C for 3 min.
Ni/Si = 1/4 (Mw+Th)-A+B (5 min)	1/4	5.5	5.09	-	184	Combined microwave & thermal treatment at 600 °C for 3 min.

Notes on notation: See Section 3 for sample identification.

3.12.2. Co/Si Catalyst

The above procedure was applied to Co/Si catalyst with a reduced scope. This catalyst was used in Fischer-Tropsch synthesis the details of which are available [8]. The XRD studies of this catalyst system indicate that when Co/Si precursor fluid ([Co]/[Si] = 1/4) was microwaved or subjected to heat treatment (at 600 °C using the Method-C, Section 3.8), it only formed Co_3O_4. When Co_3O_4 reduction was carried out at 550 °C in H_2, metallic cobalt with some CoO (without any Co_3O_4) were obtained indicating that the initial Co_2O_3 was first reduced to CoO followed by Co. Following a prolonged plasma promoted Fischer-Tropsch synthesis [47] for 150 h, Co/Si catalyst was removed and XRD

pattern was obtained which indicates oxidation of Co to CoO [8]. However, the catalyst can be reduced in-situ using the same plasma-reactor system which was used in the Fischer-Tropsch synthesis [8]. These results are collectively shown in Figure 13. However, as we have detected no reduction in catalyst efficiency, the oxidation of Co to CoO (after the removal of catalyst from the reactor for XRD analysis) is probably due to the exposure of Co catalyst to air.

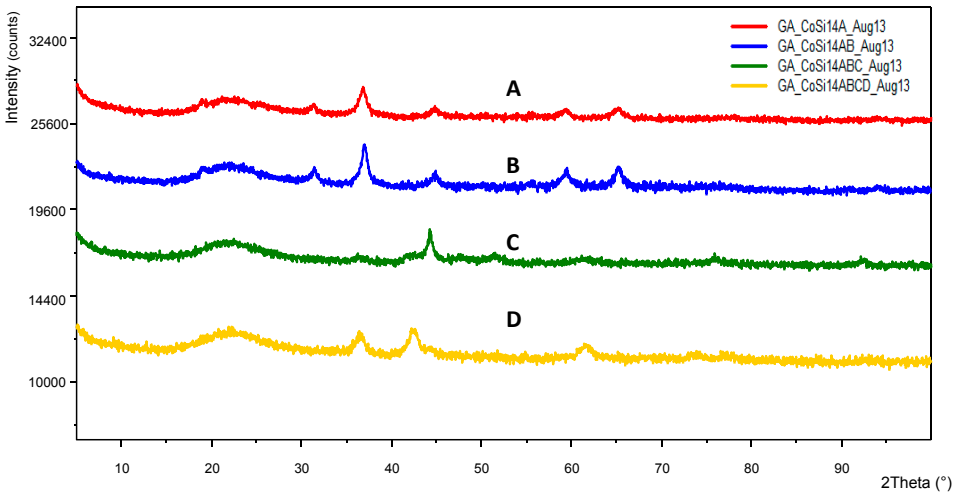

Figure 13. XRD patterns of Co/Si = 1/4 Mw at various stages of processing (**A**, **B**, **C**) and after being used for Fischer-Tropsch synthesis (**D**).

Table 2 summarizes the results for Co/Si as regards cobalt and cobalt oxide crystallite size after various treatments. In all cases, the microwave power was 1 kW. Heat treatment was at 600 °C (Method-C, Section 3.8). Reduction was at 550 °C in H_2 atmosphere for 24 h.

Table 2. Summary of XRD and BET surface area characteristics of Co/Si catalysts at various stages of processing.

Sample No. ⇩	Compound ⇨ 2θ ⇨ Sample Code ⇩	Crystallite Size (nm)			BET Surface Area (m^2/g)	Comment
		Co_3O_4 36.8°	CoO 42.4°	Co 44.3°		
1	Co/Si = 1/4 Mw-A	9.20	-	-	152	Solution Microwaved at 1 kW for 4 min.
2	Co/Si = 1/4 Mw-AB	10.1	-	-	144	Sample-1 heat treated
3	Co/Si = 1/4 Mw-ABC	-	5.01	15.6	130	Sample-2 reduced
4	Co/Si = 1/4 Mw-ABCD	-	6.21	-	N/A	Sample-3 used in FT-synthesis
Various	Co/Si = 1/5 Mw-A *	7.12 ± 0.61 *	-	-	158 ± 11	See note below *

* Note: This result is an average of 8 experiments obtained when the Etos-1 microwave reactor was used at various power ratings (0.2–1 kW) as shown in Figure 9a.

3.12.3. Ni/Si and Co/Si Catalysts from Bulk Mixing Followed by Heat Treatment

The experiments summarized above in Sections 3.12.1 and 3.12.2 all relate to the use of the catalyst precursor fluid being used in a manner, where the highly porous catalyst was obtained because of boiling/film formation during the evaporation of water. In the initial experiments in which the Haake Mixer or a GAP-Agglomerator were used, film formation was restricted because water evaporation was slow without boiling (*i.e.*, low power density). As a result, a paste-like material or dense powder was obtained. We have also used uncoated silica as a support in which a paste was obtained even at low silica concentration, thus making the use of the Haake Mixer necessary to obtain a high level of silica loading. In all cases, there was no decomposition of nitrate salt of the catalyst, except when a film was formed between the rotor and mixer wall as shown in Figure 4. This decomposition was local and the thickness of the film was *ca.* 200 μm.

A summary of these results is shown in Table 3. Here the catalyst size was calculated from XRD patters using the dominant peak for NiO (2θ = 43.2°) and Co_3O_4 (2θ = 36.8°). The XRD pattern of the uncoated silica with cobalt nitrate are shown in Figure 14. Figure 14a refers to the sample obtained after being processed in the Haake Mixer and Figure 14b refers to the sample after been heat treated at 600 °C using Method-C (Section 3.8). Figure 14a shows the loss of some crystal water from $Co(NO_3)_2$. After heat treatment, cobalt is in the form of Co_3O_4.

Table 3. Effect of processing conditions on the catalyst size and surface area, after heat treatment at 600 °C (Method-C; Section 3.8) of the samples recovered from the processing equipment (Haake Mixer or GAP-Agglomerator). Film formed between the rotor and mixer wall in the Haake mixer was recovered after the decomposition of the catalyst precursor salt as shown in Figure 4.

Processing Equipment/Section No:	Support Precursor	Catalyst System	Surface Area (m^2/g)	Catalyst Oxide Size at Dominant Peak (nm)
Haake/Bulk/Section 3.4.1	Uncoated silica	[Co]/[Si] = 1/5	218	23.3
Haake/Bulk/Section 3.4.2	Coated silica	[Co]/[Si] = 1/5	182	22.4
Haake/Film/Section 3.4.2	Coated silica	[Co]/[Si] = 1/5	191	11.7
Haake/Bulk/Section 3.4.2	Coated silica	[Ni]/[Si] = 1/5	214	18.2
Haake/Film/Section 3.4.2	Coated silica	[Ni]/[Si] = 1/5	207	9.06
Agglomerator/Section 3.5	Coated silica	[Ni]/[Si] = 1/5	238	21.1
Macro-porous nickel foam/Section 3.6	Coated silica	[Co]/[Si] = 1/4	-	20.9

It is clear from Tables 1–3 that where the film is formed, the catalyst size (after heat treatment) is 2–8 times greater compared with the case when the catalyst precursor did not form a film because of the paste-like behavior of the precursor fluid. When a film was formed during the processing using the Haake mixer, decomposition of the catalyst precursor nitrate salt took place. Although the catalyst size was reduced, nevertheless it was still significantly larger compared with the case when thin films were formed from the catalyst precursor solution during boiling. When the supported catalyst precursor fluid was placed within the pores of nickel foam and heat treated at 600 °C (Method-C; Section 3.8) in order to suppress film formation, the catalyst oxide size was also high, compared with the case when film formation was present.

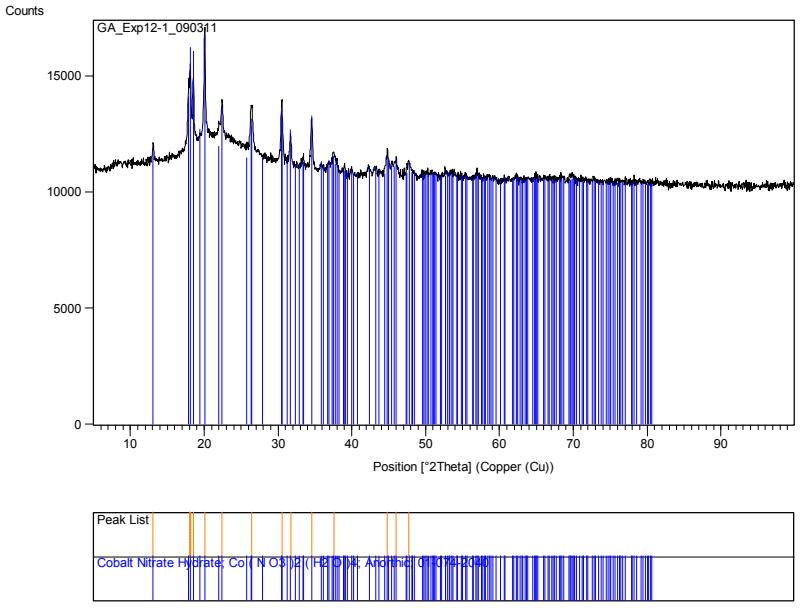

(**a**)

Figure 14. *Cont.*

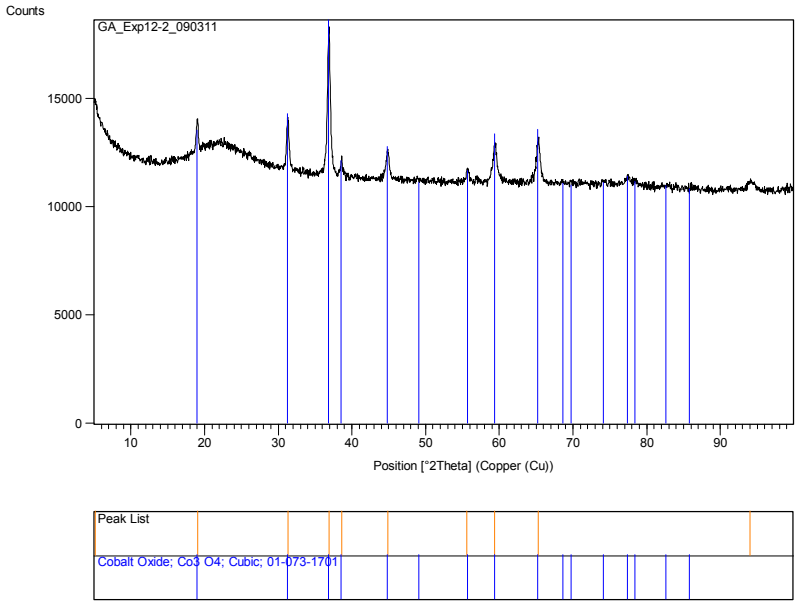

(**b**)

Figure 14. XRD pattern of the uncoated silica with cobalt nitrate (Co/Si = 1/4 Haake Mixer-Y) before and after heat treatment at 600 °C. (**a**) Sample obtained from mixing in a Haake Mixer; (**b**) After heat treatment at 600 °C using Method-C, Section 3.8 (Co/Si = ¼ Haake Mixer-YB).

3.12.4. Fe/Si Catalysts from Microwave, Thermal and Photolysis

Silica supported iron was the only catalyst system which could be obtained by using thermal- microwave- and photolysis (UV-radiation) methods. Although we have tested several other metals including Al, Mg, Ca, Co, Ni, Zn, Cu to see if they could be reduced from their nitrate salts to a corresponding oxide form in the presence of silica dispersion using UV-radiation, under the conditions used in our experiments, there was no discernable decomposition. However, in the case of $Fe(NO_3)_3$ at the UV-radiation strength of LUX = 82,000 lx, within 30 h, there was a visually observable decomposition and formation of porous magnetite flakes as confirmed by XRD provided that [Fe]/[Si] $\leqslant 1/3$. However, it was also interesting that a mixed Fe/*N*/Si (*N* = Mg, Ca, Mn; those that were tested) system does in fact yield reduced FeO. However, it appears from XRD results that the size of the crystallites associated with the second metal are very small as they are undetectable. This behavior is common in all cases when Fe with or without a second metal and the supported catalyst precursor fluid was reduced using UV, microwave irradiation or thermal treatment. Nevertheless, TEM studies indicated that the Fe/N/Si binary systems had the same nano-structure as Fe, Co and Ni. The samples (Fe/N/Si or Fe/Si) in each category were brought together and their X-ray diffraction patterns were analyzed, which revealed that they contained un-decomposed nitrate. Therefore, these samples were washed in de-ionized water and then subjected to surface area, XRD, SEM and TEM analysis. These results are shown in Figure 15.

Figure 15a shows the XRD-pattern of the 120 h of UV-irradiated (at LUX = 82,000 lx, 25 °C and 50% relative humidity) Fe/Si sample (Fe/Si = 1/4 Ph-A) before and after wash when Fe_3O_4 peak at $2\theta = 35.2^\circ$ became sharper. Figure 15b is the XRD pattern of Fe/Mn/Si = 1/1/8 Ph-A sample after 120 h of photolysis under the same conditions as the above sample, Fe/Si = 1/4 Ph-A. Apart from the silica peak at $2\theta = 21.9^\circ$, Figure 15b shows two broad peaks at $2\theta = 33.1^\circ$ and $2\theta = 35.2^\circ$ identified as $FeFe_2O_4$ (magnetite) and Fe_2O_3 (hematite) respectively. Figure 15c is the XRD-pattern of the sample Fe/Mn/Si = 1/1/8 (Mw+Th)-A+B obtained after the combined Microwave and Thermal treatment at 600 °C for 2 min. The broad peak at $2\theta = 35.5^\circ$ refers to $MnFe_2O_4$.

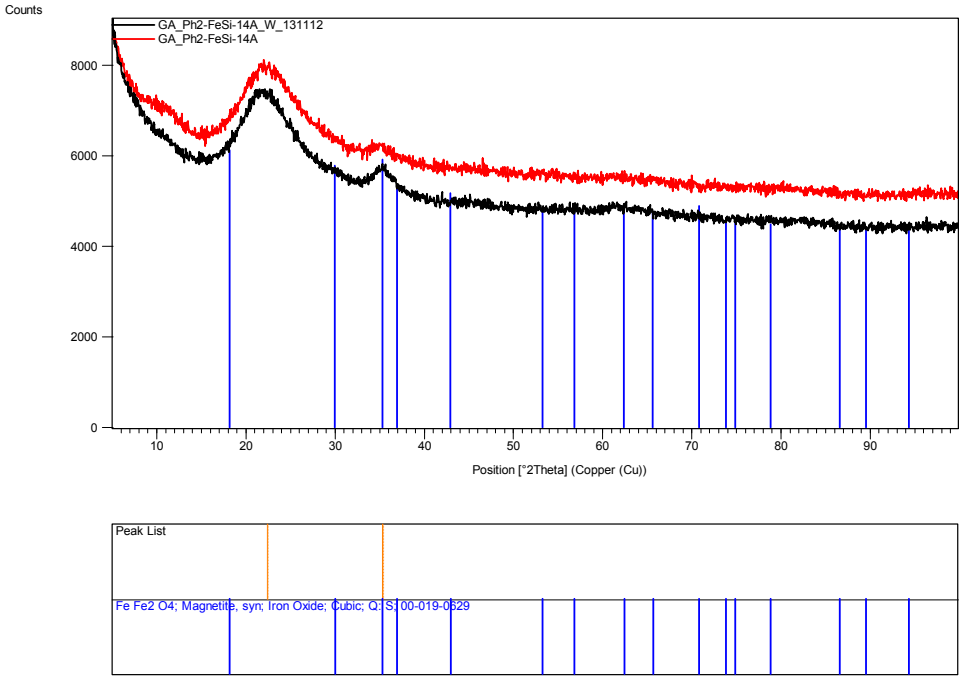

(**a**)

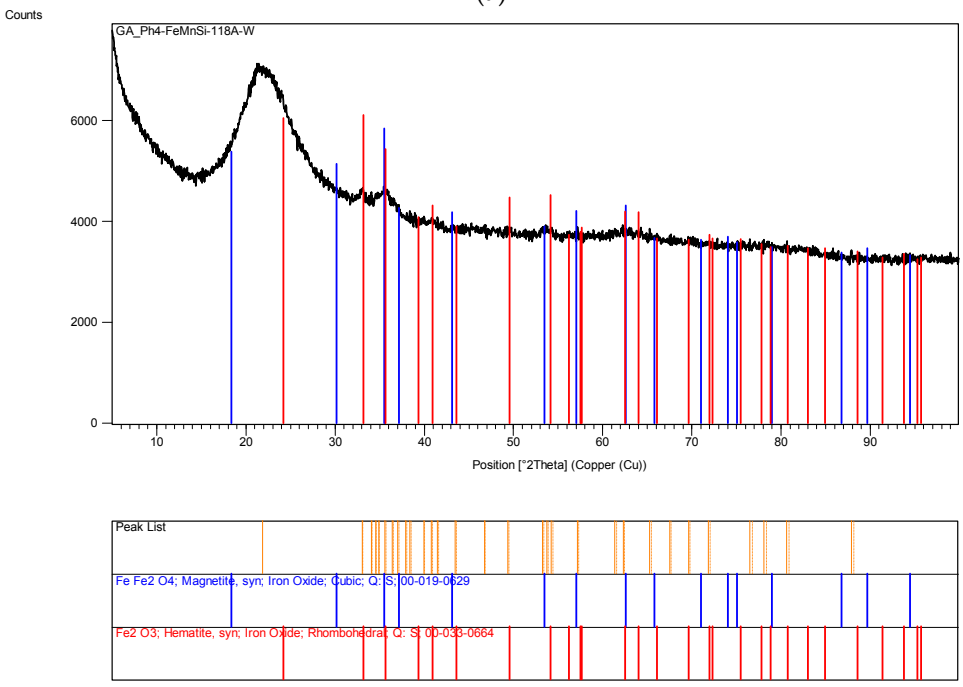

(**b**)

Figure 15. *Cont*.

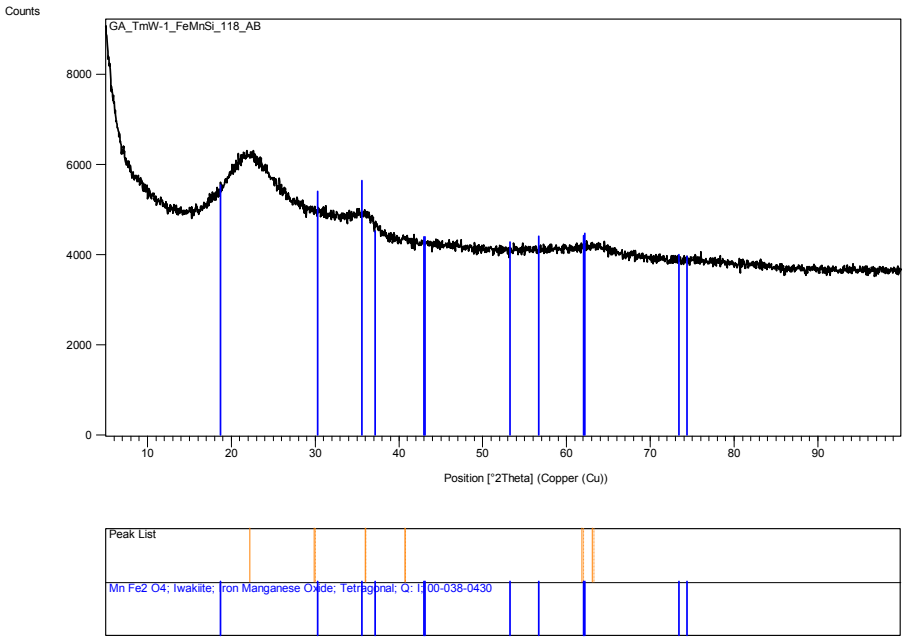

(**c**)

Figure 15. XRD patterns of iron based silica supported catalyst systems obtained from 120 h of UV-radiation at LUX = 82,000 lx, 25 °C and 50% relative humidity using an agricultural growth cabinet (**a**,**b**) or under combined microwave and thermal treatment (**c**). Glass beakers (50 mL capacity) were used to contain 20 mL supported catalyst precursor fluid to obtain flakes of the supported catalyst.

(a) Fe/Si = 1/4 Ph-A before and after washing of the UV-irradiated samples to remove unreacted $Fe(NO_3)_3$. Peaks match $FeFe_2O_4$ (magnetite).

(b) Fe/Mn/Si = 1/1/8 Ph-A catalyst system after washing. Peak ID-bars match $FeFe_2O_4$ (Magnetite) as well as Fe_2O_3 (Hematite) although they are very broad.

(c) Fe/Mn/Si = 1/1/8 (Mw+Th)-A+B catalyst system after combined microwave and thermal treatment of the supported catalyst precursor fluid for 120 s at 1 kW microwave power and 600 °C followed by rapid cooling in air. XRD peak identification bars refer to iron manganese oxide ($MnFe_2O_4$).

Table 4 summarizes the surface area of various samples indicating that all samples have a very large surface area with no significant variation in surface area as a result of composition or the method. We also included the surface area of Fe/Si sample which was prepared using a microwave oven at 1 kW (Fe/Si = 1/4 Mw-A). Also included is the Fe/Mn/Si = 1/1/8 (Mw+Th)-A+B supported catalyst system processed through combined thermal and microwave irradiation at 600 °C for comparison with the photo-irradiated silica supported iron catalyst samples. Table 4 shows that the surface area of these samples are similar while the analysis of the XRD data indicate that the crystallite size is *ca.* 1–3 nm range.

Table 4. Variation of surface area of photo-catalyzed silica supported iron catalysts. See Section 3 for the notation of the sample identification.

Sample ID	Fe/Si = 1/4 Ph-A (washed) Method-1	Fe/Si = 1/4 Ph-A (washed) Method-2	Fe/Si = 1/4 Mw-A	Fe/Ca/Si = 1/1/8 Ph-A (washed) Method-1	Fe/Mn/Si = 1/1/8 Ph-A (washed) Method-1	Fe/Mn/Si = 1/1/8 (Mw+Th)-A+B
Surface Area (m^2/g)	267 *	254 *	303	240 *	268 *	233

* Notes: See Section 3.10 for Methods-1 and 2.

3.13. Scanning Electron Microscopy (SEM) Studies

SEM and TEM studies were carried out in order to illustrate the structure of the catalyst and derive some conclusions about the possible mechanism of catalyst generation with a novel catalyst structure. However, this process required the examination of several hundreds of SEM and TEM images of the samples produced under different conditions with different catalysts. In the case of SEM studies, all the samples were sufficiently conductive so that coating with carbon or gold was not necessary thus allowing an accurate evaluation of the fine structure as well as EDX analysis when needed, provided that the magnification was below *ca.* 50,000. At magnifications above, the catalyst samples had to be coated with gold. It was also found that the TEM images of all the catalysts studied (namely Ni, Co, Fe) were similar, provided that they were produced through film formation from the catalyst/support precursor fluid containing the catalyst precursor nitrate and silane coated silica.

Figure 16 illustrates the SEM of a Co/Si = 1/5 (Haake Mixer, uncoated silica) catalyst when it was produced from the highly viscous uncoated silica dispersion using the Haake Mixer followed by calcination at 600 °C as described in Section 3.4.1. These images show a highly dense structure. Although it had a very large surface area of 218 m^2/g; dominant cobalt oxide crystallite size (23.3 nm) was also very large as summarized in Table 4.

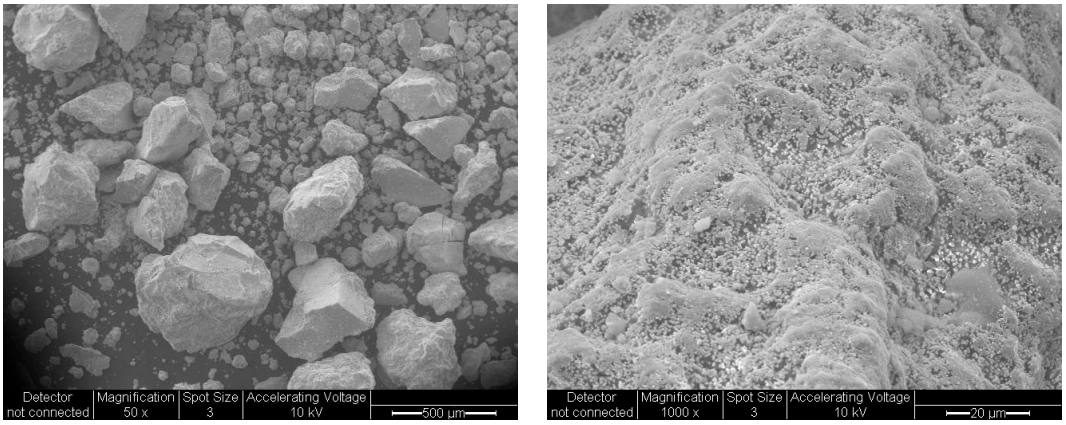

(**a**) (**b**)

Figure 16. Scanning electron microscopy of sample Co/Si = 1/5 using uncoated silica and processed using the Haake Mixer (Section 3.4.1) followed by heat treatment at 600 °C using Method-C; (Section 3.8) at two magnifications. (**a**) Scale bar = 500 µm; (**b**) Scale bar = 20 µm.

When coated silica dispersion (Bindzil CC30) was used as the catalyst support precursor to obtain solid supported catalyst particles in which the Haake Mixer was the processing equipment (Section 3.4), more porous overall structure was obtained as shown in Figure 17. This SEM image is for Co/Si = 1/5 after it was heat treated at 600 °C using Method-C (Section 3.8). The surface area of this sample was 182 m^2/g and the crystallite size was 22.4 nm.

Figure 18 illustrates the highly porous structure of Co/Si = 1/4 Mw-AB catalyst which was obtained from the microwave irradiation of catalyst/support precursor fluid at 1 kW followed by heat treatment at 600 °C (Method-C, Section 3.8). Figure 18a shows the micro-porous structure while Figure 18b illustrates the wall structure which indicates the presence of large surface pores and flower-like structures surrounded by boundary-lines. The flower-like patterns are further illustrated in Figure 18c. It can be seen from Tables 1–4 compared with Ni and Fe, the crystallite size of Co/Si is significantly large. This is partly because Co appears to prefer to be located at the precursor fluid/air interface by breaking through the silica surface. This results in "unconstrained" crystallite growth as discussed further in Section 3.16.

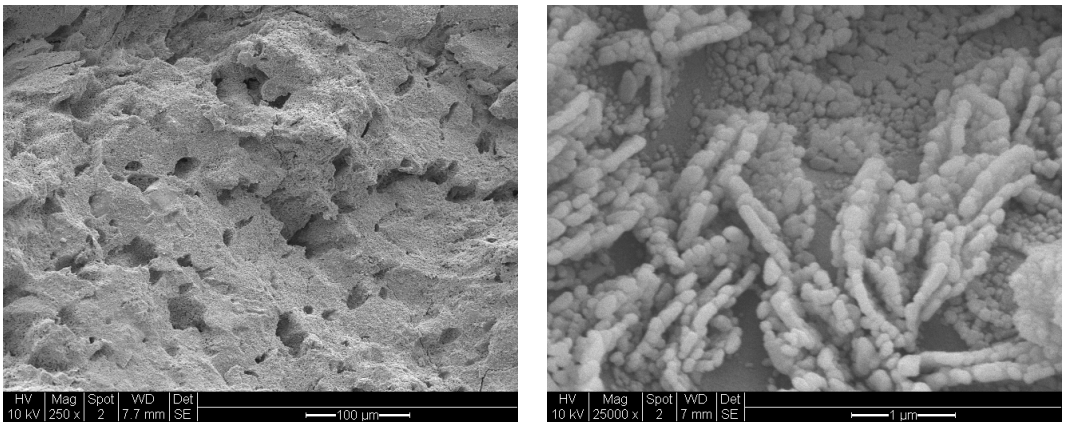

(**a**) (**b**)

Figure 17. Scanning electron microscopy of sample Co/Si = 1/5 (using silane coated silica and processed using the Haake Mixer, Section 3.4, followed by heat treatment at 600 °C using Method-C; (Section 3.8) at two magnifications). (**a**) Scale bar = 100 µm; (**b**) Scale bar = 1 µm.

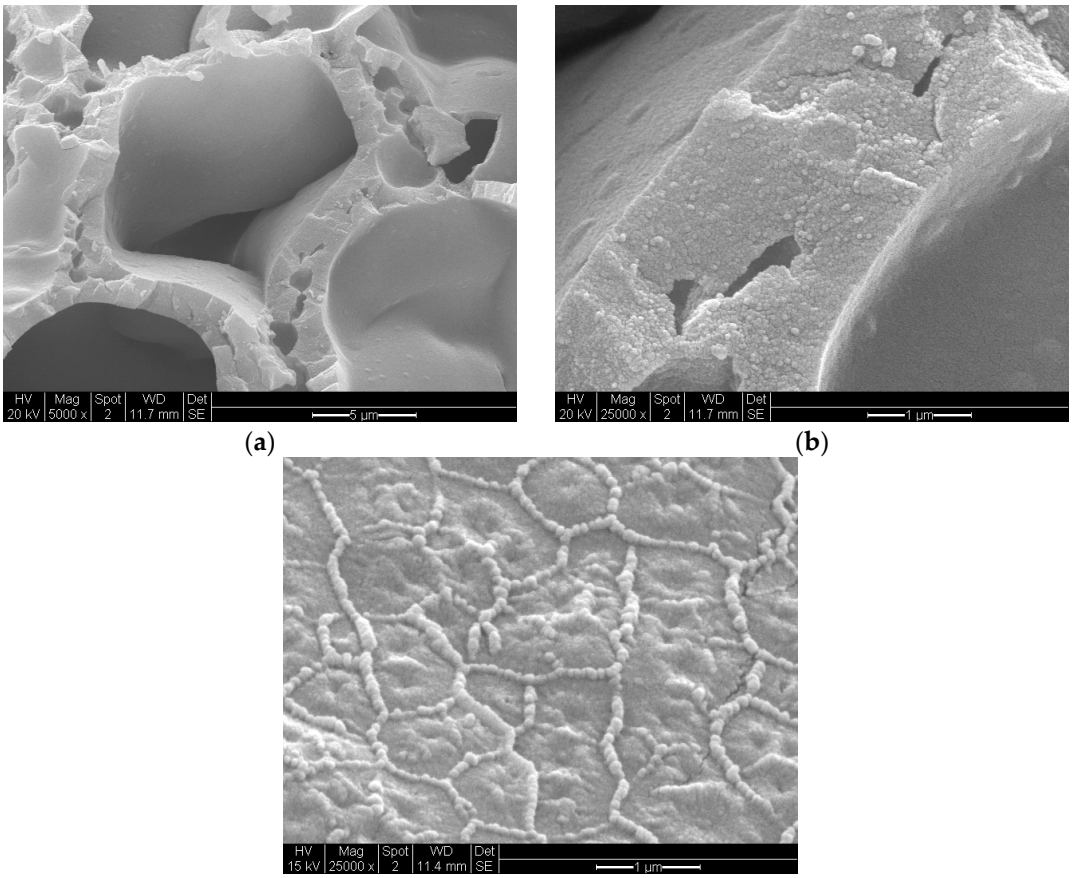

(**a**) (**b**)

(**c**)

Figure 18. Scanning electron microscopy of sample Co/Si = 1/4Mw-AB obtained after the microwave irradiation at 1 kW of supported catalyst precursor fluid to obtain Co_3O_4 followed by heat treatment at 600 °C (Method-C, Section 3.8). (**a**) Porous structure (Scale bar = 5 µm); (**b**) Wall structure (Scale bar = 1 µm) and (**c**) Surface structure (Scale bar = 2 µm). Characteristics of this catalyst system are summarized in Table 2.

Figure 19 illustrates the porous structure of Ni/Si = 1/4 Mw-AB catalyst which was obtained from the microwave irradiation of catalyst/support precursor fluid at 1 kW followed by heat treatment at 600 °C (Method-C, Section 3.8). Figure 19a shows the micro-porous structure while Figure 19b illustrates the wall structure. The surface of the catalyst walls (*i.e.*, air/fluid interface during processing) are also porous with significant reduction in surface pores compared with that obtained for Co/Si = 1/4Mw-AB. However, it is possible to obtain larger pores and larger wall pores by using chemical blowing agents incorporated in to the supported catalyst fluid [8].

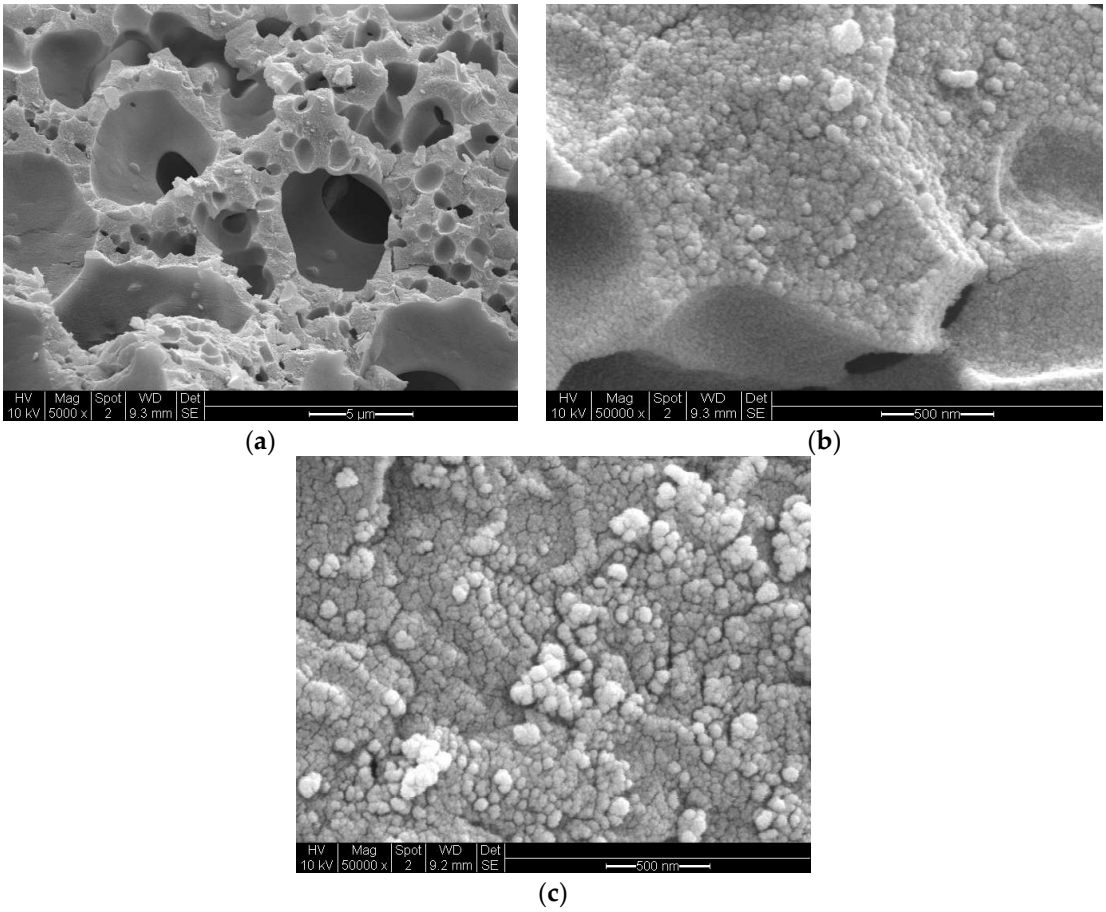

Figure 19. Scanning electron microscopy of sample Ni/Si = 1/4 Mw-AB obtained after the microwave irradiation at 1 kW of supported catalyst precursor fluid to obtain NiO followed by heat treatment at 600 °C (Method-C, Section 3.8). (**a**) Porous structure (Scale bar = 5 µm); (**b**) Wall structure (Scale bar = 500 nm); (**c**) Surface structure (Scale bar = 500 nm).

Figure 20 illustrates the structure of a Fe/Si = 1/4 Ph (washed) sample obtained through UV-irradiation of the precursor fluid for 120 h followed by washing in water. Figure 20a is the overall structure and Figure 20b is the wall structure. Although the structure of the Fe/Si = 1/4 Ph is highly porous, the connectivity is through meso-pores (Figure 20a). The main structure is in the form of strands.

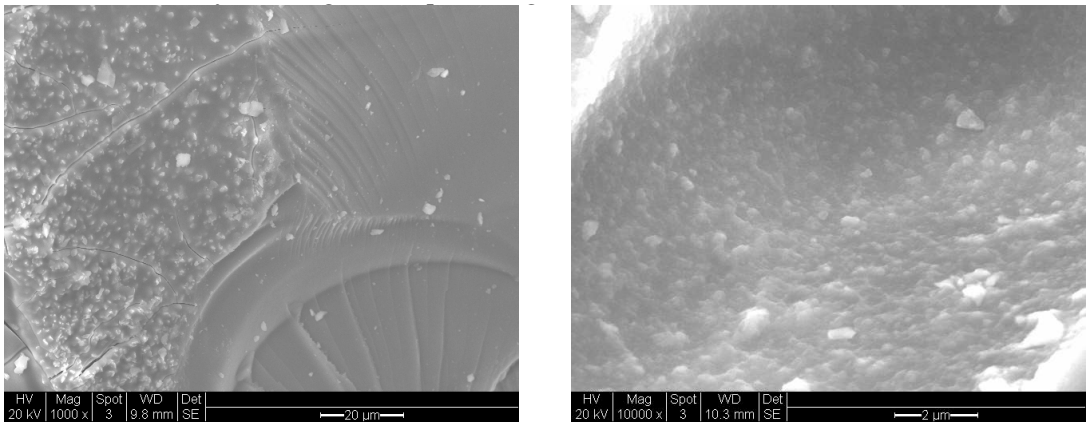

(**a**) (**b**)

Figure 20. Scanning electron microscopy of the catalyst Fe/Si = 1/4 Ph-washed, supported catalyst obtained after UV irradiation (intensity LUX = 82,000 lx) for 120 h at 25 °C and 50% relative humidity followed by washing in water at room temperature. (**a**) Overall structure (Scale bar = 20 µm); (**b**) Wall structure (Scale bar = 2 µm).

3.14. Transmission Electron Microscopy (TEM) Studies

SEM studies yield accurate images of the overall catalyst structure but they do not reveal anything about the catalyst shape, catalyst size and its distribution or any possible interactions with the catalyst support. Therefore, we have examined TEM images in order to evaluate these characteristics and to understand how they were formed under different processing conditions for different catalyst compositions. It was found that there is no single nano-structure associated with these catalysts but there are some common structures shared by all the catalysts studied. The heterogeneity of nano-scale structure is not surprising since small dynamic changes or driving forces at nano-scale can cause extensive spatial and time variations in the catalyst structure. Furthermore, recent advances in high resolution and sensitivity spatiotemporal spectroscopy also reveal that the heterogeneous catalysts behave almost like living-objects [48]. However, the dominant nano-structures are dependent on the processing conditions as well as the catalyst composition. The sizes of the nano-structures are also dependent on the catalyst composition and catalyst preparation history.

Figure 21 shows nearly all of the nano-structures encountered throughout this study. Here the catalyst (Co/Si = 1/4 Mw-ABC) was prepared by microwave irradiation of the catalyst/support precursor fluid for 4 min at 1 kW to obtain Co_3O_4, followed by heat treatment at 600 °C using Method-C (Section 3.8). Co_3O_4, was then reduced by hydrogen for 24 h at 550 °C. However, it was observed from the TEM images that there were no significant changes in the catalyst nano-structure after the initial catalyst oxide formation. The BET and XRD analysis of the sample after the reduction stage gave BET = 130 m^2/g and XRD based catalyst size was 15.6 nm evaluated at $2\theta = 44.3^\circ$ as the dominant peak corresponding to metallic cobalt while CoO size at $2\theta = 42.4^\circ$ was 5.01 nm (See Table 2).

Figure 21 shows a large (measuring *ca.* 250 nm × 100 nm × 20 nm) closed ellipsoidal structure with wall thickness of *ca.* 20 nm. It can also be observed that the wall of this structure has a bar-code type of printing representing the catalyst. This figure also shows several polyhedral structures in the form of rods or irregular shapes. These structures also contain layered detail similar to bar-codes observed in the case of the large ellipsoidal structure. We have collected a number of similar structures from other samples produced by thermal, microwave or photo-radiation or by combined thermal and microwave radiation. These TEM images illustrate the dominant structures in all the samples examined and presented in Figures 22–24.

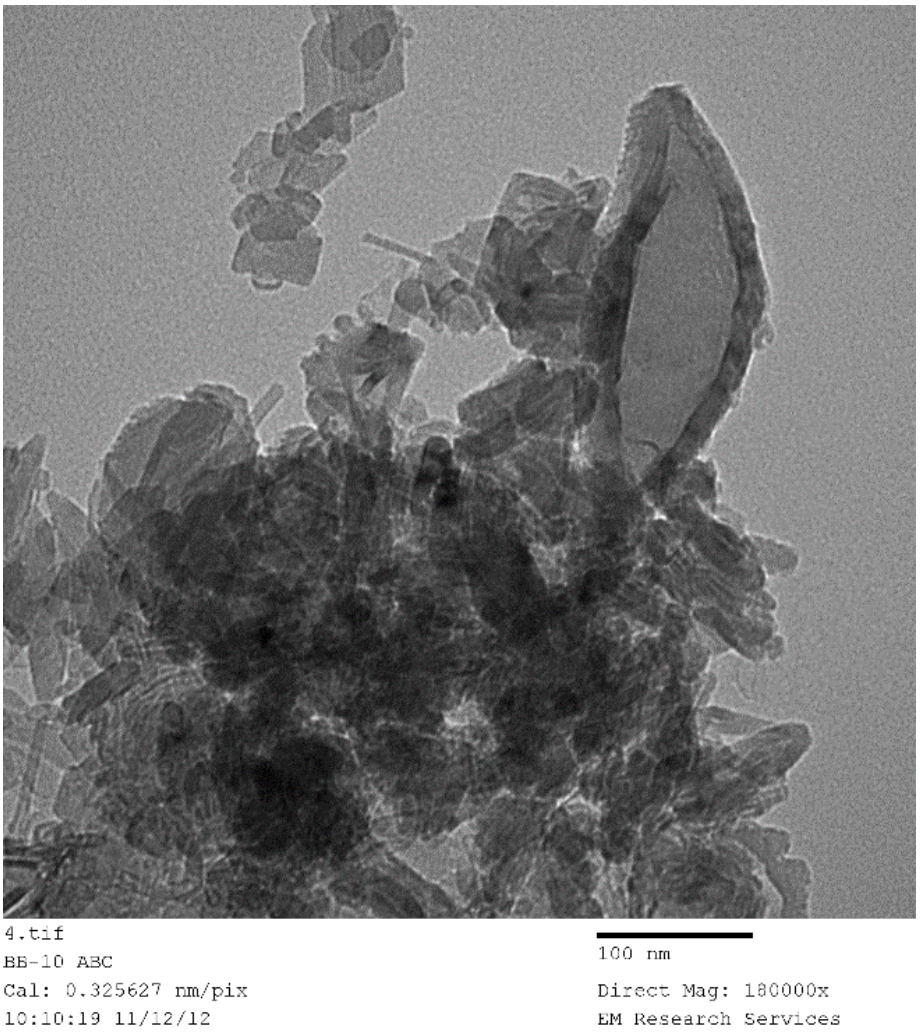

Figure 21. Transmission electron microscopy image of silica supported cobalt catalyst produced through microwave irradiation followed by heat treatment at 600 °C and then reduced in a hydrogen environment at 550 °C. Sample is coded as Co/Si = 1/4 Mw-ABC. Scale bar = 100 nm.

The basic bar-code type structure for several samples of differing catalysts and process history is shown in Figure 22a–f. Figure 22a,b illustrates a very long (1100 nm) and thick (20 nm) rectangular rod with a bar-code-like catalyst structure. This catalyst is coded as Ni/Si = 1/4 Mw-ABCD, indicating the catalyst history: The supported catalyst precursor fluid was microwaved at 1 kW, followed by heat treatment at 600 °C and then reduced in hydrogen at 550 °C and finally used in ammonia synthesis using a low temperature plasma reactor [46]. The enlarged view of this structure is shown in Figure 22b. The bar-code strips in this structure are rather irregular compared with other structures in general as seen in Figure 22c–f. The catalyst history for these samples are given in the figure caption for Figure 22. This difference is due to the fact that the bar-code strips are highly concentrated and they also overlap. The width of the bar-code strips can be as small as 0.6 nm (see Figures 22c and 23d) but in general, they are approximately 2 nm. These strips of catalyst are separated by silica support with similar width. The height of the bar codes is also variable, ranging from a few nanometers to 20 nm. As for the length of the bar-code strips, it appears to be highly variable. Examination of several images show that they can be very small (*ca.* 1 nm) but can reach *ca.* 20 nm. It is difficult to be accurate since overlapping small bar-code strips can give the impression of continuity of the catalyst sheet.

As seen from Figures 21–24 these bar-code structures are common in all of the catalysts systems irrespective of the type of energy used for processing, including UV-radiation as observed in

Figure 23c,d. Figure 22e,f indicates that the processing using combined energy fields do not influence the catalyst structure. In Figure 22e combined microwave and thermal energy were used (2 min) whereas, microwave and ultra-sound (US) were combined in the production of the sample in Figure 22f. However, the dimensions of the ribbons with bar-code strips/plates can be controlled in two ways. If the pH of the catalyst/support precursor solution is reduced from its natural pH (= 5.5) to pH = 0.2 with the addition of nitric acid, the ribbon dimensions are drastically reduced as seen in Figure 22d. In this case, the microwave irradiation of the catalyst precursor fluid did not result in the decomposition of the nitrate salt but a green porous solid structure was obtained. When this porous supported precursor structure was heat treated at 600 °C, the resulting supported catalyst (Ni/Si = 1/4 Mw-YB) had very large crystallite size (43.3 nm) as also apparent from Figure 12b. Alternatively, if the energy input is too high, (*i.e.*, combined Thermal (Th) and Microwave (Mw) radiation), the overall dimensions of the ribbons are also reduced as seen in Figure 22e.

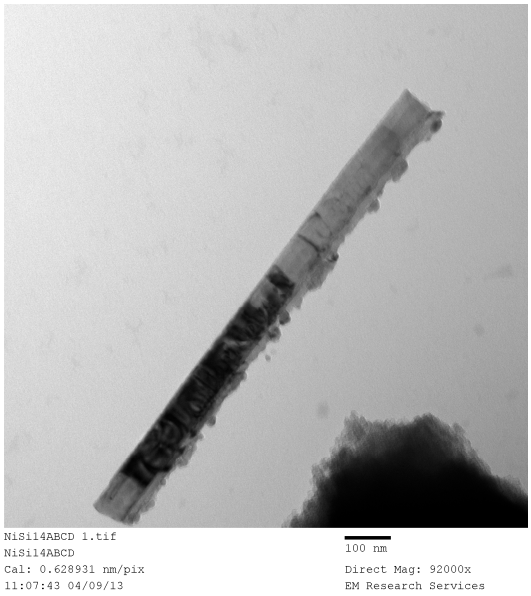

(**a**)

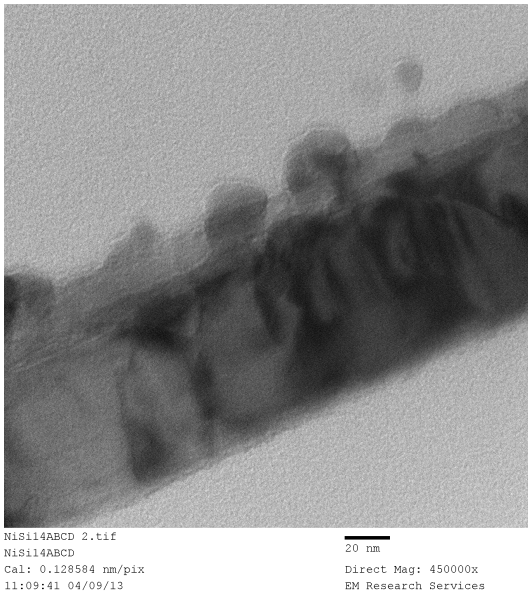

(**b**)

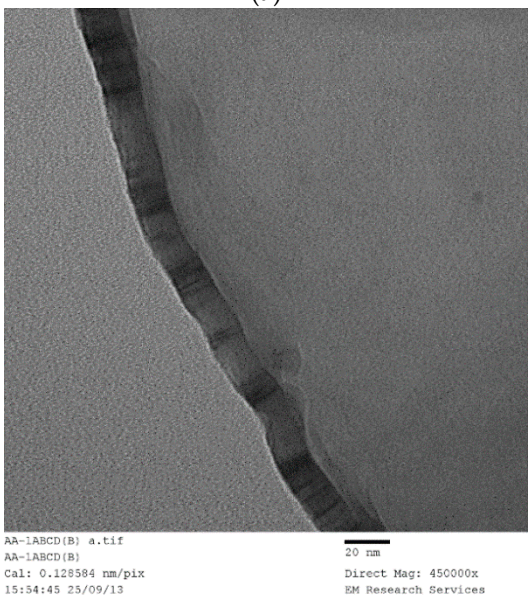

(**c**)

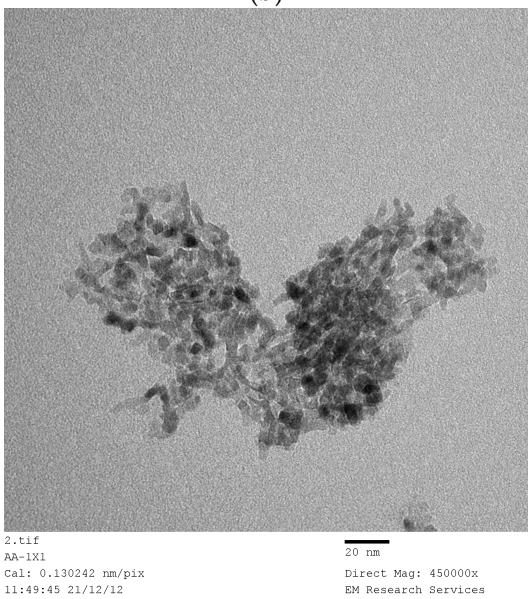

(**d**)

Figure 22. *Cont.*

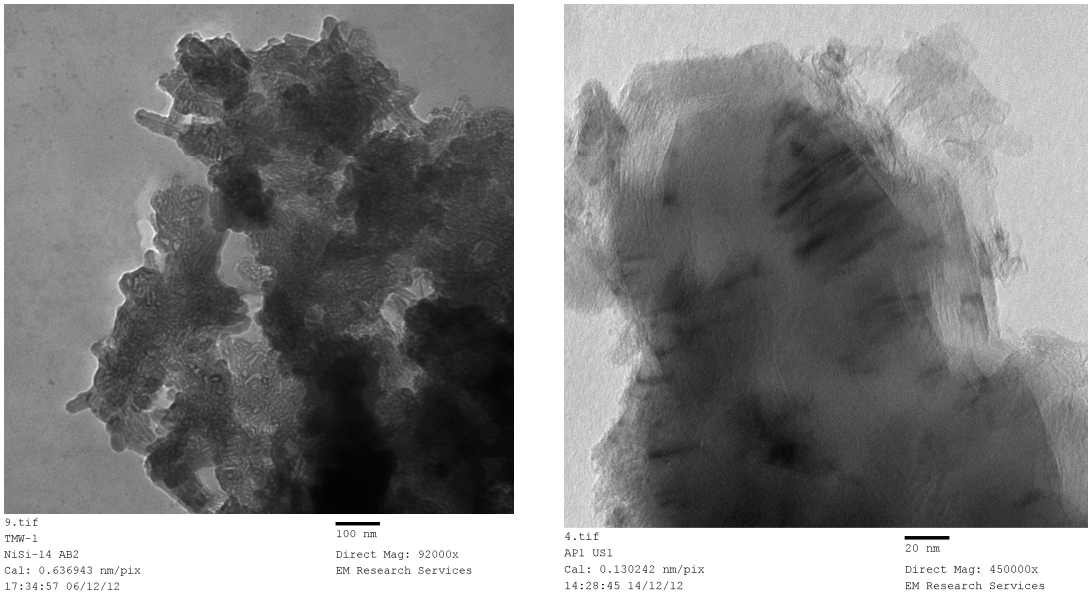

(**e**) (**f**)

Figure 22. TEM images of several Ni/Si catalysts with varying compositions and processing history. (**a**) Ni/Si = 1/4 Mw-ABCD (Bar = 100 nm); (**b**) Ni/Si = 1/4 Mw-ABCD (Bar = 20 nm); (**c**) Ni/Si = 1/4 Mw-ABCD (Bar = 20 nm); (**d**) Ni/Si = 1/4 Mw-Y pH = 0.2 (Bar = 20 nm); (**e**) Ni/Si = 1/4(Mw+Th)-A+B (Bar = 100 nm); (**f**) Ni/Si = 1/5(Mw+US)-A (Mw = 0.4 kW; US = 0.04 kW) (Bar = 20 nm).

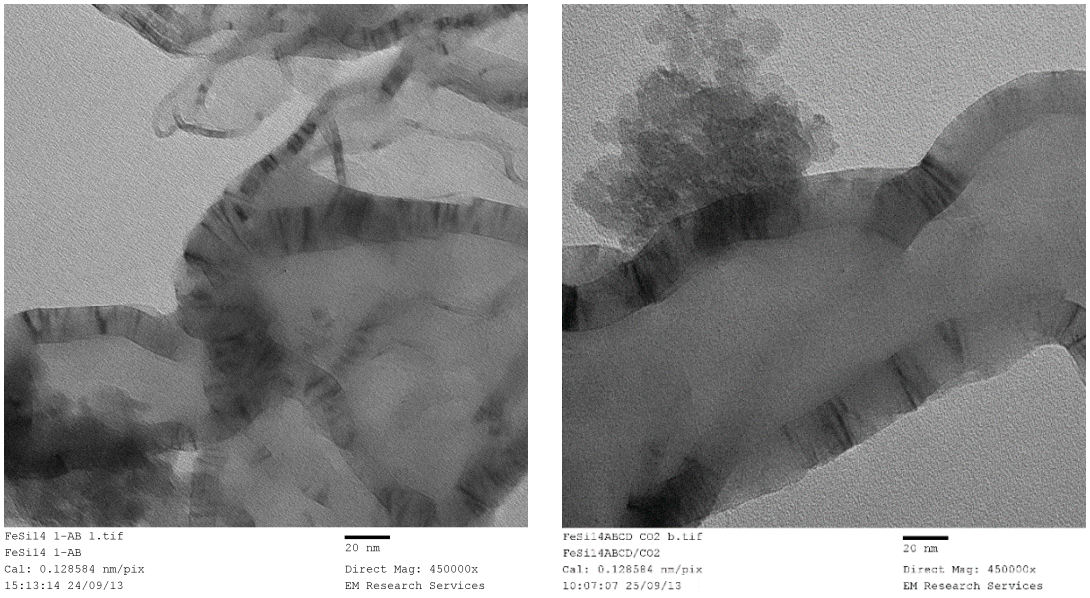

(**a**) (**b**)

Figure 23. *Cont*.

Figure 23. TEM images of several Fe/Si and Fe/Mn/Si catalysts with varying compositions and processing history. (**a**) Fe/Si = 1/4 Mw-AB (Bar = 20 nm); (**b**) Fe/Si = 1/4 Mw-ABCD (Bar = 20 nm); (**c**) Fe/Si = 1/4 Ph-washed (Bar = 20 nm); (**d**) Fe/Mn/Si = 1/1/8 Ph-washed (Bar = 20 nm).

The ribbons with bar-code strips can co-assemble to form lamellar structures as shown in Figure 22f similar to lyotropic surfactant lamellar sheets based on surfactant bilayers. However, these self-assembly lamellar sheets are interrupted by defects as a result of mis-orientation or presence of large lamellae. When the lamellae with dense bar-code strips overlap, they will appear as dense and irregular catalyst depositions in TEM images as seen in Figure 24a. In this figure, two disk-like particles (size 50 nm and 130 nm) with bar-code strips can be identified, together with several other more dense particles. For this reason, it is important to investigate the catalyst structure at very high magnifications with images taken from several areas of the TEM sample. Figure 24b also shows particles which would appear as large dense catalyst particles at low magnifications, giving the impression that the catalyst size is very large. Here too, the catalyst structure is in the form of concentric lamellae also encountered in some lyotropic surfactant systems. In some cases, the catalyst structure appears as an aggregation of small particles next to the bar-code structures as seen in Figures 22d and 23b.

Therefore, the catalyst size cannot be evaluated from the TEM images due to the heterogeneity of the catalyst structure, and that the catalyst particles are not spherical but in the form of lamellae. Although XRD based evaluation of the catalyst size yields a quantitative measure, in view of the various structures encountered in this study, it is not clear how these catalyst sizes relate to the actual size and its distribution.

Clearly, the TEM images presented in Figures 21–24 show that the catalyst system presented in this study is fundamentally different from those prepared by wash-coating or deposition methods where a high surface area solid support (such as alumina, zeolites, silica, nano-tubes and rods) is impregnated by the catalyst precursor and subsequently reduced, leaving a deposit of metal catalyst particles on the solid support or in its pores. In the present case, both the catalyst and the support precursors are in liquid form and both are transformed to solid after the evaporation of water and subsequently heat treated/reduced to obtain the catalyst. The catalyst and the support therefore interact at the liquid state and the catalyst forms nano-scale lamellar structures in the form of bar-code strips or thin sheets separated by the support material. Therefore, the catalyst surface area per unit weight of catalyst is significantly higher compared with the catalyst generated through deposition

methods. Furthermore, the catalyst loading is high while the accessibility of the catalyst is provided by hierarchic pore structure. The presence of lamellar structure with alternate catalyst-support layers, also prevents the enlargement of the catalyst when the supported catalyst is subjected to high temperatures.

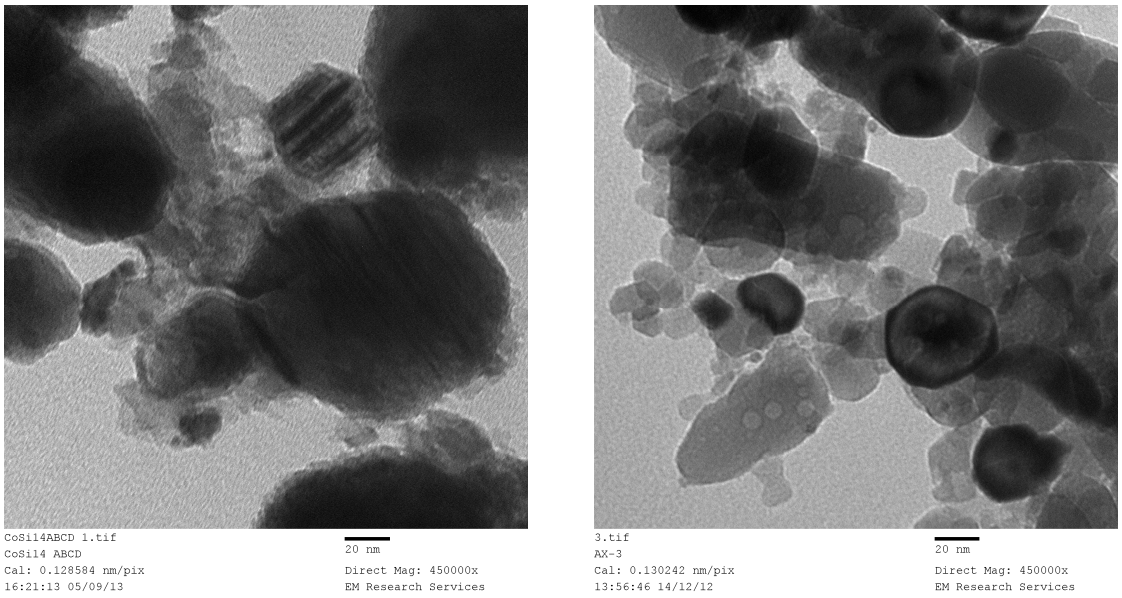

(**a**) Co/Si = 1/4 Mw-ABCD (**b**) Ni/Si = 1/2 Mw-YB

Figure 24. TEM images of Co/Si and Ni/Si catalysts with varying compositions and processing history showing the presence of planar (**a**) or spherical layering (**b**) of the catalyst.

As seen from the foregoing presentation, we have considered various methods of processing in order to establish the best technique as well as to understand the mechanism of catalyst generation by the current method. The techniques which do not allow the generation of porous catalyst/support precursor result in dense catalysts with significantly large catalyst size which also increases with increasing catalyst loading. Furthermore, if the catalyst loading is above a threshold for a given power input, conversion from supported catalyst precursor fluid to catalyst oxide/support does not take place. Therefore, microwave-radiation or photo-radiation can only be applied to certain catalysts below a certain catalyst loading. In this case, thermal treatment of the catalyst/support precursor needs to be applied with or without microwave/photo-radiation.

3.15. Summary of Catalyst Characteristics

In this study, our objectives are to obtain an efficient supported catalyst system and establish its mechanism of generation. Promising catalysts developed here have been successfully applied to Fischer-Tropsch synthesis [45], dry reforming [45] and ammonia production [46]. However, in these studies, we have not optimized the catalyst properties for a given purpose, such as, selectivity or conversion. In these studies, we have considered the catalyst size, catalyst loading and the surface area of the catalyst system. Furthermore, in order to evaluate the mechanism of catalyst formation and to be able to compare the results obtained using different methods, we have adopted a heat treatment procedure in which the supported catalyst oxide obtained from microwave or UV-radiation were heat treated at 600 °C using Method-C (Section 3.8) which resulted in an increase in catalyst oxide size. This treatment is also necessary in order to burn-off the coating on the catalyst surface before the catalyst reduction at 550 °C in a hydrogen atmosphere. In the case of the thermal method, heat treatment is part of the film/bubble generation process as well as subsequent removal of the coating on the silica support.

In some cases, the removal of the organic coating can be carried out at low temperatures (*ca.* 150–250 °C), using low temperature Dielectric Discharge Plasma in the presence of oxygen [8,45] followed by reduction using hydrogen in the same plasma reactor. This process stops size enlargement at high temperatures.

However, the advantage of thermal treatment is that at high catalyst loading, higher microwave power is needed and the thermal process is a single step process for the catalyst oxide formation and removal of coating on silica. Clearly, if the catalyst support is preferred to be carbon, catalyst reduction can be carried out using nitrogen in a low temperature plasma reactor to carbonize the silica coating, followed by catalyst reduction.

Here, we summarize the variation of the Ni/Si catalyst surface area and catalyst size before they are ready for reduction using hydrogen. In each case, supported catalyst precursor fluid was used to obtain supported catalyst oxide. Figures 25 and 26 show the variation of catalyst surface area and catalyst size (based on XRD) with catalyst loading (catalyst molar fraction) defined as [Ni]/([Ni]+[Si]) as a function of processing condition, to investigate if microwave radiation before heat treatment has any beneficial effect.

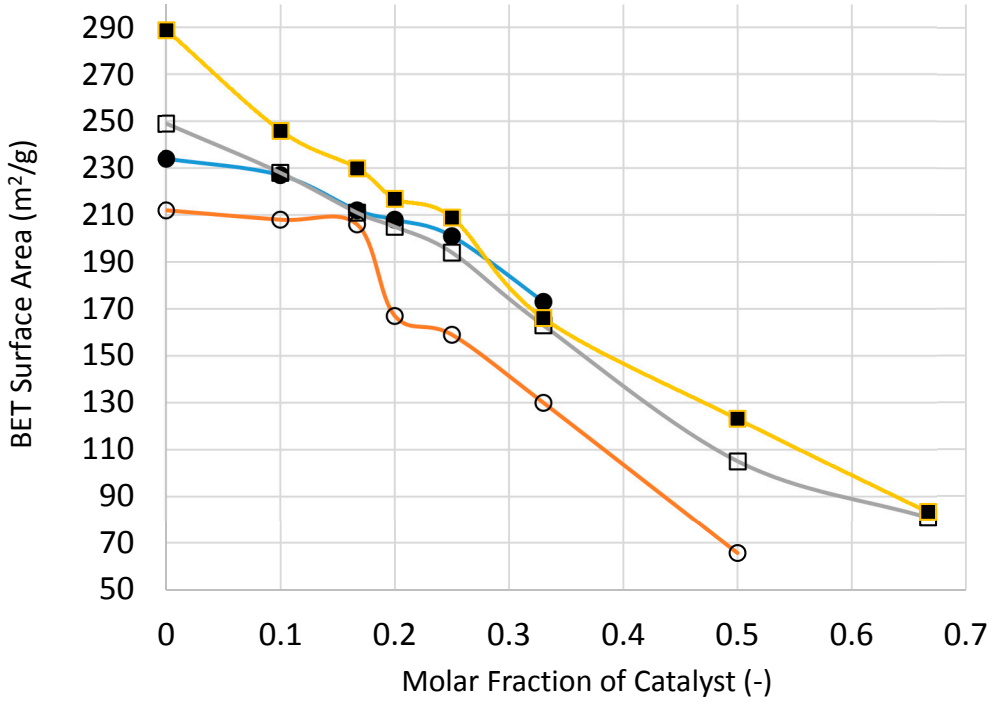

Figure 25. The effect of catalyst loading on the surface area of the supported nickel catalyst system before reduction with hydrogen after the formation of NiO. (●)—Microwave radiation at 1 kW (Stage-1a); (○)—Thermal processing at 300 °C with slow heating and slow cooling using Method-A, Section 3.8 (Stage-1b); (□)—Thermal processing at 600 °C with fast heating and fast cooling using Method-B, Section 3.8 (Stage-1c); (■)—Thermal processing at 600 °C with slow heating and slow cooling using Method-C, Section 3.8 (Stage-1d).

Figure 25 indicates that the catalyst loading reduces the catalyst/support surface area which increases with increasing processing temperature as well as the duration of heat treatment. The reduction in surface area becomes less marked with increasing catalyst loading except when the heat treatment is at 300 °C. Surface area reduction with catalyst loading is partly due to increased density of the supported catalyst system. Nevertheless, microwave irradiation appears to yield higher surface area at high catalyst loading which can be attributed to smaller catalyst size, as indeed shown in Figure 26.

If the density increase due to catalyst loading is taken into account, it can be shown that the surface area of the catalyst system in fact increases. Instead of using surface area per unit weight as a quantitative measure of surface area, a more realistic measure is in fact surface area per unit volume, or surface area density, measured in m^2/m^3. The importance of surface area density in heat and mass transfer processes is well known and for this reason it is also described as Transfer Area Density [17]. In Figure 25, the measured BET surface area of the silica support for the microwaved sample is 234 m^2/g. When $[NiO]/[SiO_2]$ = 1/3 the BET surface area of the catalyst is 173 m^2/g. Assuming densities of 2.20 g/cm^3 for amorphous SiO_2 and 6.67 g/cm^3 for NiO, the corresponding surface area densities are 5.15 × 10^8 m^2/m^3 for SiO_2 support and 6.32 × 10^8 m^2/m^3 for the catalyst system (Ni/Si = 1/3 Mw-A), indicating some 20% increase in surface area of the catalyst oxide.

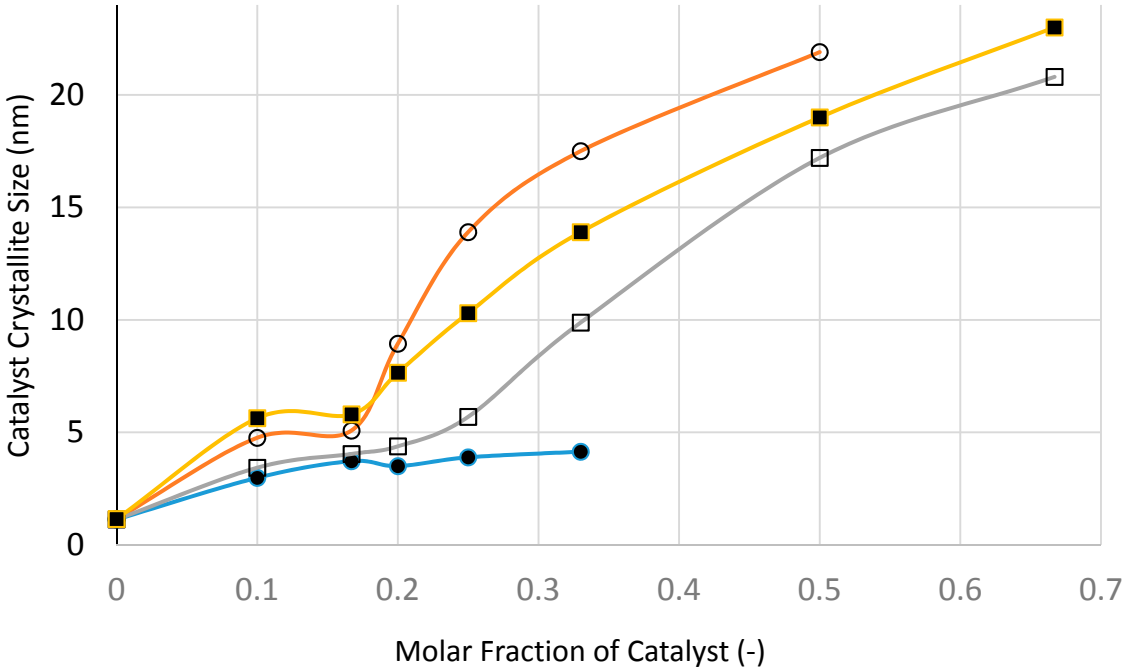

Figure 26. The effect of catalyst loading on the XRD-based catalyst size of the supported nickel catalyst system before reduction with hydrogen after the formation of NiO. (●)—Microwave radiation at 1 kW (Stage-1a); (○)—Thermal processing at 300 °C with slow heating and slow cooling using Method-A, Section 3.8 (Stage-1b); (□)—Thermal processing at 600 °C with fast heating and fast cooling using Method-B, Section 3.8 (Stage-1c); (■)—Thermal processing at 600 °C with slow heating and slow cooling using Method-C, Section 3.8 (Stage-1d).

The variation of XRD-based catalyst size with catalyst loading shown in Figure 26 indicates that at all catalyst loadings, microwave processing provides smaller catalyst size when compared with the other processes, especially at high catalyst loadings. Even after taking into account a slight increase in catalyst size following heat treatment at 600 °C using Method-C (see Table 1), the microwave method still provides the smallest catalyst size.

Not surprisingly, fast heating and fast cooling at 600 °C is to be preferred to slow heating/slow cooling process at 600 °C. What is surprising is that the heat treatment at 300 °C provides by far the largest catalyst size compared with other methods. Below the catalyst loading of 20 mol %, the difference between all of the methods is not as marked as they are at high catalyst loadings. At this catalyst loading, the precursor fluid is able to form film/bubbles, a process which is hindered at high catalyst loading due to the decrease of silica concentration. Processing at 300 °C benefits from low temperature when the catalyst growth is hindered. However, at high catalyst loading, film formation is hindered (also due to low temperature) and hence the processing becomes similar to that with

suppressed film formation. This is also true for fast heating and fast cooling at 600 °C which enhances film formation and suppresses catalyst aggregation due to prolonged heat treatment.

Microwave processing provides the best method, even if it is necessary to have a separate heat treatment stage (*i.e.*, Method-C) to burn off the catalyst coating. If this is the case, the combined microwave and thermal process is the best option as it is also suitable as a continuous process. Furthermore, if a carbon support is needed for the catalyst, initial microwave decomposition followed by carbonization under an inert atmosphere provides a viable route.

3.16. A Tentative Mechanism of Catalyst Structure Development

Although the primary aim of this study is to produce supported catalysts with a high surface area and small and controlled catalyst size having a hierarchic pore size distribution for use in heterogeneous catalysis, we have also carried out experiments in order to illustrate the mechanism of catalyst system generation which appears to be novel and generic.

As demonstrated above, the micro- and nano-structure formation in the silica supported catalysts, including the mixed catalyst, is generic. The basic nano-structure in the form of bar-codes does not depend on the processing history and the processing energy source. However, at a constant catalyst loading, the catalyst size is strongly dependent on the way in which the supported catalyst system is prepared. In all cases, the catalyst system is prepared from a precursor dispersion of silica and catalyst precursor nitrate salt solution which is referred to as "Precursor Fluid". If the catalyst support silica is not coated, the precursor dispersion is a highly viscous paste-like material which needs to be processed by using high-torque internal mixers, commonly encountered in polymer processing. If the support silica is coated to reduce the dispersion viscosity, the resulting dispersion (at the same silica concentration and silica particle size) also acquires elasticity (*i.e.*, high elastic modulus and extensional viscosity) as a result of which coated silica dispersion can form thin films. If water is gradually evaporated (instead of rapid evaporation with film boiling) during mixing of the coated silica support with catalyst precursor nitrate solution for impregnation, a highly viscous, paste like material is also obtained.

The most important factor in the generation of small catalyst size and hierarchic pore structure is the ability of the catalyst precursor liquid to form film or bubbles. The bubble/film formation during microwave, UV-radiation or thermal treatment of the precursor fluid is clearly observable during processing. At this stage, the proto-catalyst structure is formed and as water is evaporated rapidly from the film, the proto-catalyst structure is frozen and when the film collapses back in to the precursor fluid it keeps its integrity because the air-liquid interface is stabilized by silica particles. These nucleated structures are sufficiently stable not to revert to a dispersion state. This conclusion is in line with the observations made for the pendant drop experiments described in Section 3.1.

The evidence of bubble formation with a stabilized interface is also available from the TEM-images as shown in Figures 21 and 23a–d as well as in Figure 27. The bubble seen in Figure 27 is in the form of an extended ellipsoid measuring some ca. 770 × 140 nm. The bubbles present in Figure 21, Figure 23a–d and Figure 27 contain a number of smaller bubbles, presumably captured during the chaotic period of bubble formation and collapse. The thickness of the bubble wall is *ca.* 20 nm which appears as a ribbon as seen in Figure 22a–c as well as in Figure 21, Figure 23a–d and Figure 27.

The bar-code structure (presented in Figure 22a,b) measuring ca. 1100 nm × 80 nm is formed from the fracture of a large ellipsoidal bubble wall. When such semi-solid structures emerging during film formation aggregate through random packing, they form micro-porous structures. The overall micro-porous structure is best observed through SEM. However, due to the magnification limitations of SEM especially those associated with semi-conductors such as silica-metal oxides, it is not possible to reach the magnifications levels of TEM to observe the bar-code structures. Coating of these catalysts with a conductor will mask the inherent bar-codes. Reduction of the catalyst to enhance conductivity is a possibility, but due to oxidation of the metal during handling and the inherent semi-conductor nature of the catalyst, high resolution/magnification SEM investigation is not possible.

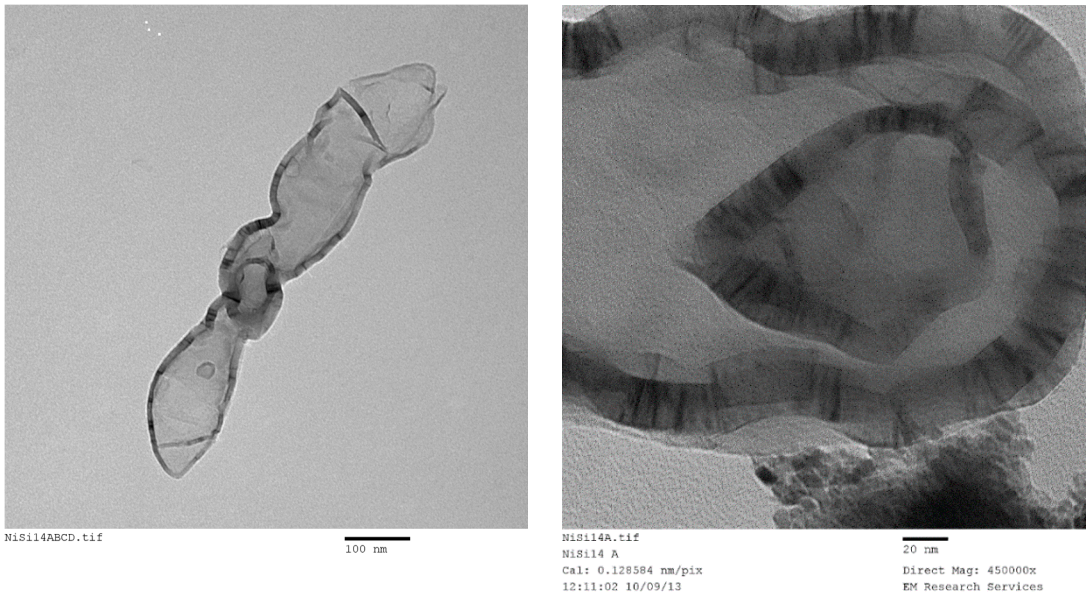

(**a**) (**b**)

Figure 27. Presence of a complete elongated bubble in Ni/Si precursor fluid formed as a result of silica/nickel interaction during the boiling stage of the precursor fluid. (**a**) Complete bubble from Ni/Si = 1/4 Mw-ABCD (used in ammonia production). Scale bar = 100 nm; (**b**) Enlarged view of two bubbles from the catalyst oxide Ni/Si = 1/4 Mw-A. Scale bar = 20 nm.

In order to observe the presence of the ribbon structure under SEM, it is however possible to obtain large planar structures grown from the self-associated ribbons. One such system was found to be Co/Cu/Si = 1/1/8 Mw-A system ([Co]/[Cu]/[Si] = 1/1/8 so that ([Co]+[Cu])/[Si] = 1/4). The high magnification SEM images of this sample after microwave irradiation are shown in Figure 28. In this binary catalyst system, there is a separation into Co and Cu rich phases. In these flower-like structures, the atomic composition was Co/Cu/Si = 1/1.44/3.12 as determined by EDX analysis. These flower-like structures are formed from planes with thickness in the range of *ca.* 50 nm–200 nm, although the large structures are clearly formed from thinner planes. The length of the large planes can be as high as 1 micron. These observations are shown in Figure 28a–c. As seen in Figure 28a,b, the planar structures appear to grow as they emerge from the walls of the catalyst wall which is dominantly silica rich (Figure 28c,d). These flower-structures fade when the binary catalyst is heat treated at 600 °C as in fact shown in Figure 18c.

The walls in the form of ribbons have a surface skin layer of silica with thickness *ca.* 2 nm as seen from Figures 22c,f and 23b. However, there is no evidence of the presence of the 7 nm silica particles anywhere in the TEM images of the silica systems investigated. In fact, these particles were conspicuously absent on the walls of the ellipsoidal bubbles or between the catalyst strips/planes forming the bar-code appearance in the ribbon structures. Spherical silica particles only appear occasionally (Figure 24b), but their size is often below 7 nm. The absence of the original catalyst support particles and formation of planar bar-code structures with catalyst/silica separation as low as 0.6 nm should be explained in the mechanism of present catalyst preparation technique.

The apparent absence of silica particles in the catalyst structure can be explained if we consider that the primary silica particles revert back to the proto-silica particle state. The fumed silica is obtained through flame pyrolysis of silicon tetrachloride. After the generation of SiO_2 molecules, they form proto-particles which are subsequently enlarged (aggregated) to form the stable primary silica particles with size 4 nm or above. These particles can be further agglomerated for some applications. Particle size reduction in nano-silica can be considered to be similar in mechanism to de-lamination of glass

which occurs due to the imposition of thermal stresses enhanced by a chemical environment including the presence of electrolytes [49–52].

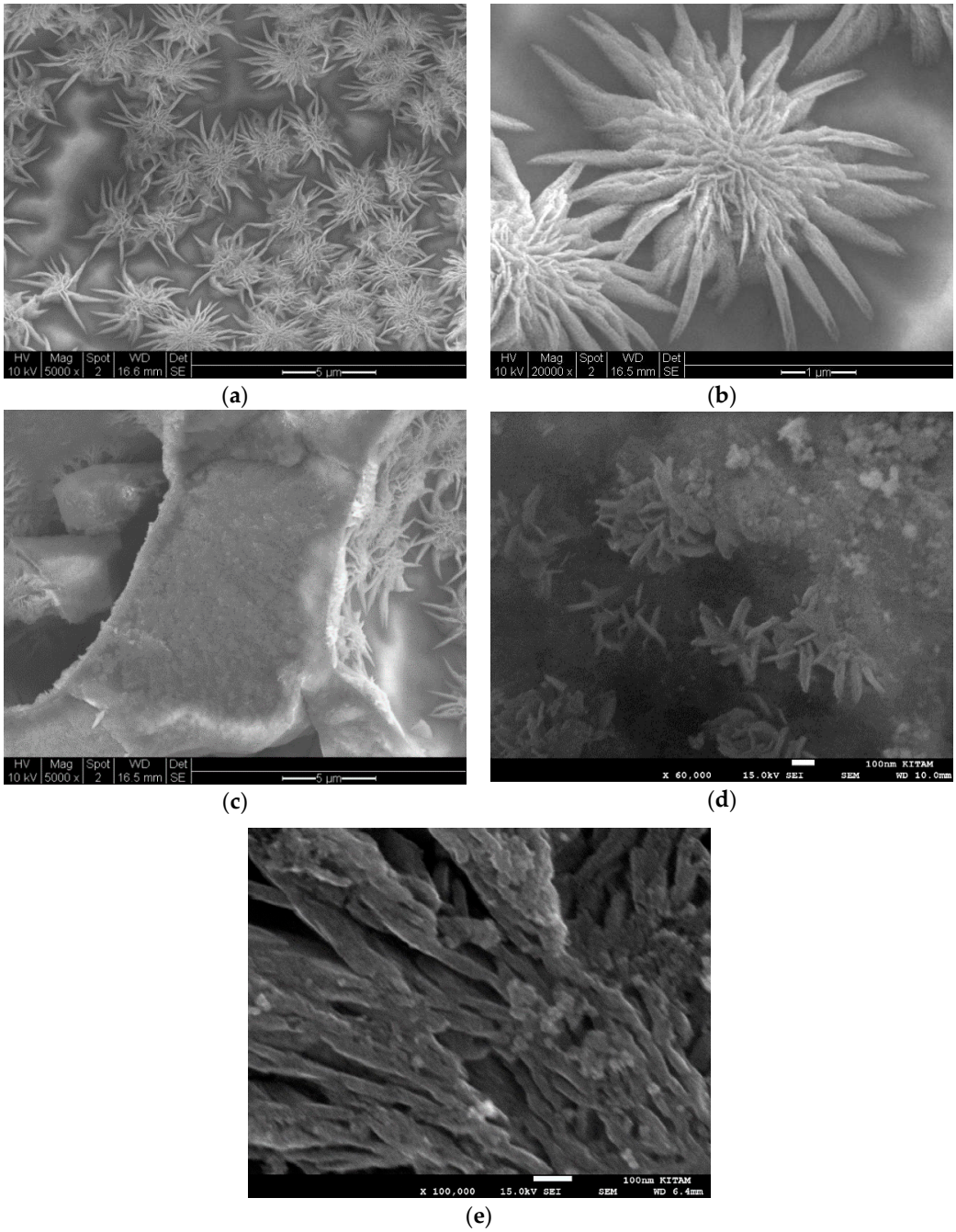

Figure 28. Structure of Co/Cu/Si = 1/1/8 Mw-A binary catalyst system showing the presence of planar aggregates formed at the catalyst/air interface during the microwave irradiation (1 kW) of supported binary catalyst precursor fluid. (**a**) Wall surface structure (Scale bar = 5 µm); (**b**) Wall surface structure at higher magnification (Scale bar = 1 µm); (**c**) Wall cross-section structure (Scale bar = 5 µm); (**d**) Enlarged view of the wall cross-section structure showing the presence of phase separation in the form of proto-flower structures (Scale bar = 100 nm); (**e**) Long ribbons of supported catalyst formed from the films/elongated bubbles during boiling of the precursor fluid. These strips are several hundreds of nanometers long and *ca.* 40 nm wide form a porous wall structure of the catalyst (Scale bar = 100 nm).

Figure 29 illustrates TEM image of $Fe(NO_3)_3$ in coated silica dispersion at a molar ratio of [Fe]/[Si] = 1/3 after 30 h of UV-radiation in the agricultural growth cabinet (see Section 3.10). The liquid sample was taken before the formation of solid flakes of Fe_3O_4/SiO_2 as described in Section 3.10. Figure 29 illustrates three features;

1. Presence of some spherical particles with size *ca.* 7 nm (*i.e.*, primary silica particles) which appear to be coated by iron
2. Larger elongated rectangular particles, and
3. Bar-code structures with varying size and metal-silica regions.

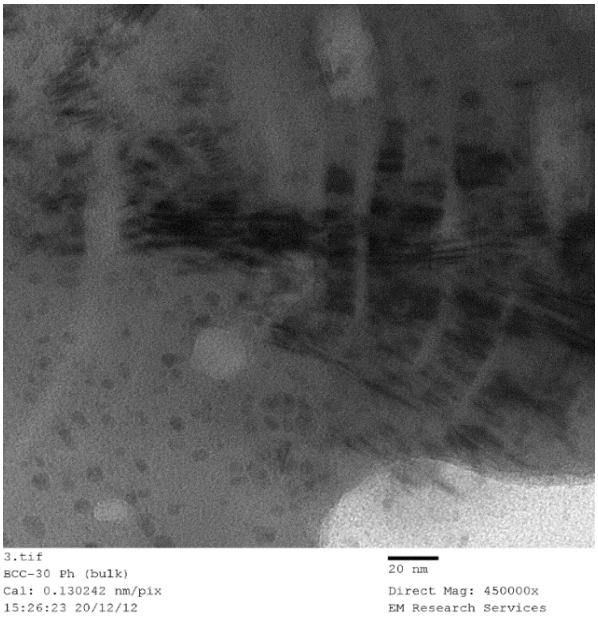

Figure 29. TEM image of the catalyst/support precursor fluid (Fe/Si = 1/4 Ph) after UV-irradiation for 30 h. It shows the de-aggregation of the silica particles and the formation of liquid crystal phases in the form of bar-codes.

Figure 29 illustrates the possibility of nano-scale de-lamination which should probably be better described as molecular de-aggregation under radiation. Therefore, we can assume that the same process occurs during supported catalyst formation as a result of microwave, thermal or ultrasound radiation or indeed when these processing vectors are combined.

Following the formation of these basic ordered liquid crystal structures which in fact appear to have a similar structure to lyotropic (surfactant-water liquid crystal systems) lamellar self-assembly [53,54] as well as molecular liquid crystals in smectic phase [55]. It is likely that this structure is formed at the air-liquid interface but remains intact once the interface structure returns back into the solution. This is also true for the lyotropic lamellar phase; once formed, these surfactant assemblies can remain stable for months even after dilution in water when they are expected to form micelles before the thermodynamic equilibrium is established [53,54]. It is likely that the smectic phase appearance of the ordered structures in Figure 29 is due to the presence of proto-silica particles with silane coating and those without any silane coating.

This assumption is in agreement with the optical rheometry observations when a bubble is formed at the tip of a syringe and irradiated by light to measure the response of the bubble to the changes in its volume. In the presence of $Fe(NO_3)_3$, bubble response was a solid-like behavior indicating that the air/liquid interface has been stabilized with a network of silica.

During microwave or thermal or UV-radiation of the catalyst precursor liquid, the liquid films/bubbles are formed. These structures are stabilized by the formation of the bar-code structures at

the air-liquid interface. However, during this process, water evaporates thus generating hollow bubbles. These bubbles form a highly porous structure when the evaporation is complete. Subsequently, the decomposition of catalyst precursor starts provided that the energy density is sufficient for a given catalyst system.

Essentially, this decomposition takes place within nano-scale reactors in the form of porous walls formed by the bar-code ribbons. As seen in Figure 9, catalyst precursor salt decomposition in fact takes place at significantly lower temperatures (*ca.* 140 °C) compared with the decomposition in the absence of coated silica. The temperature programmed pyrolysis of cobalt nitrate and support precursor dispersion (Figure 3) also shows that the decomposition was detected at 90 °C whereas, cobalt nitrate without coated silica starts decomposition at *ca.* 200 °C. Furthermore, the TGA study shown in Figure 2 shows that when [Co]/[Si] $\leqslant 1/2$, initially, the weight loss is faster than the weight loss from the cobalt nitrate solution. Figure 2 further shows that the mechanism of decomposition is also different in the presence of coated silica as indicated by the weight loss steps in TGA. In the pyrolysis study (Figure 3), nitric oxide evolution profiles of cobalt nitrate with or without coated silica show that not only NO evolution starts at a lower temperature but the amount of NO evolved is far in excess in the presence of coated silica. This can be understood in terms of reduced oxygen availability since the nitrate salt is essentially encapsulated by silica and hence decomposition results in more NO rather than NO_2.

Table 3 summarizes the characteristics of the silica supported catalysts obtained without the film/bubble formation. In this case we used primarily the Haake high torque mixer which was supplemented by an agglomeration method and also by catalyst generation within the pores of nickel foam. In all cases, the resulting catalyst was dense and the catalyst size was large, at least 2–4 fold of corresponding catalysts obtained through film/bubble formation. However, when a film is formed between the rotor and stator of the Haake internal mixer, the decomposition of the catalyst precursor takes place locally (see Figure 4). Therefore, the yield is very small. As seen from Table 3, when film formation and decomposition occur, the resulting catalyst size is reduced compared with the catalyst obtained from the bulk of the mixture. Although this process is unlikely to be useful, it nevertheless shows the importance of film formation in obtaining small crystallite catalysts.

4. Conclusions

The processing, characteristics and a tentative mechanism of a novel generic supported catalyst system are described. Both the processing and characteristics of the catalyst system are fundamentally different to the currently available supported catalyst systems. The current technique can be best described as 'co-assembled supported catalyst generation'. Based on extensive XRD, SEM and TEM studies, we have evaluated the structure-processing relationships in the supported catalyst system.

We used epoxide functional silane coated 7 nm diameter silica as catalyst support and nitrate salts of Fe, Co and Ni as the primary catalyst precursors and Ca, Mn and Cu as the precursor for the binary catalyst system in illustrating the nature of the catalyst and in the evaluation of the mechanism of catalyst generation. We also used uncoated silica for comparison. Processing was carried out using several different pieces of equipment and techniques in which microwave, thermal or solar energy simulant (using an agricultural growth cabinet) were used as processing energy. Coated silica was in a low shear viscosity dispersion capable of forming film because of its high extensional viscosity (high storage modulus/elasticity). Film formation during processing is essential for the generation of highly porous (with density 0.2 g/cm^3) structure and small (*ca.* 1–10 nm) catalyst size as evaluated by XRD measurements. As determined by TEM studies, the nano-structure of the catalyst is primarily in the form of flat sheets and strips with a thickness of *ca.* 0.6–2 nm separated by the support silica. Therefore, the structure can be described as lamellar which commonly appears as a bar-code structure in TEM images. The length of lamellar structures range from *ca.* 5 nm to several hundred nanometers.

The importance of film formation in obtaining small catalyst size was demonstrated by suppressing film formation in which the catalyst was formed in the pores of metal foam, or by

using un-coated silica which cannot form a film, or by using mixing equipment to obtain a dense catalyst support/catalyst precursor mixture, followed by calcination. Catalyst size in the absence of film formation is ca. 2–4 times higher compared with catalyst obtained through film processing. However, although very high (typically 250–150 m^2/g depending on the catalyst loading), the surface area of the catalyst does not appear to depend on the processing route, because the catalyst/support surface area is mainly dictated by the support.

We have also given a tentative mechanism of supported catalyst generation to explain the structure formation as described above. This mechanism is consistent with the behavior of pendant drop of the catalyst precursor/coated silica during elastic modulus measurement. This mechanism explains why the nano-structure of the catalyst system is independent of the processing vectors; microwave, thermal and UV-radiation.

According to this model, during processing, silica support particles undergo delamination to the proto-primary particle state and form lamellar structure with the catalyst precursor during the film-forming stage of processing when water is also evaporated. These films solidify and return back to the solution but retain their porous structure. Catalyst nitrate salt then undergoes decomposition within the solidified films which essentially act as a co-assembled nano-reactor. The decomposition takes place at significantly lower temperatures and through a different reaction pathway compared with the decomposition without silica. Following the heat treatment at 600 °C to remove the organic coating, the pre-decomposition nano-structure essentially remains unaltered although the XRD-based catalyst size measurements indicate a small increase in catalyst size.

The advantages of the current technique for supported catalyst preparation include rapid (within seconds if required, using combined thermal and microwave radiation) continuous processing, scale-up and energy efficiency. The advantages of the catalyst structure achieved through this technique via co-assembled nano-reactors include small catalyst size (*ca.* 2 nm thick), high surface area, hierarchic pore structure and resistance to agglomeration/size enlargement due to lamellar structure in which the catalyst layers are sandwiched between the support material.

Acknowledgments: The research contained in this work was supported by two EU Framework Programme-7 projects (COPIRIDE, Grant agreement No: CP-IP 228853 and POLYCAT, Grant agreement No: CP-IP 246095) in which the author was the principal investigator and the director of research at Newcastle University, UK. The research was completed and further extended by another EU-grant administered by the Turkish Scientific Technical Research Council, TUBITAK (Grant No BIDEB 2236). The author thanks for these supports and his research staff as well as partners in the EU FP7 projects.

Conflicts of Interest: The author declare no conflict of interest.

References

1. Munnik, P.; de Jongh, P.E.; de Jong, K.P. Recent developments in the synthesis of supported catalysts. *Chem. Rev.* **2015**, *115*, 6687–6718. [CrossRef] [PubMed]
2. Gutierrez, L.-F.; Hamoudi, S.; Belkacemi, K. Synthesis of gold catalysts supported on mesoporous silica materials: Recent developments. *Catalysts* **2011**, *1*, 97–154. [CrossRef]
3. Casula, M.F.; Corrias, A.; Pashina, G. FeCo-SiO_2 nanocomposite aerogels by high temperature supercritical drying. *J. Mater. Chem.* **2002**, *12*, 1505–1510. [CrossRef]
4. Sietsma, J.R.A.; Meeldijk, J.D.; den Breejen, J.P.; Versluijs-Helder, M.; van Dillen, A.J.; de Jongh, P.E.; de Jong, K.P. The preparation of supported NiO and Co_3O_4 nanoparticles by the nitric oxide controlled thermal decomposition of nitrates. *Angew. Chem. Int. Ed.* **2007**, *46*, 4547–4549. [CrossRef] [PubMed]
5. Flytzani-Stephanopoulos, M.; Gates, B.C. Atomically dispersed supported metal catalysts. *Ann. Rev. Chem. Biochem. Eng.* **2012**, *3*, 545–574. [CrossRef] [PubMed]
6. Prieto, G.; Zecwvic, J.; Friedrich, H.; de Jong, K.P.; de Jongh, P.E. Towards stable catalysts by controlling collective properties of supported metal nanoparticles. *Nat. Mater.* **2013**, *12*, 34–39. [CrossRef] [PubMed]
7. Sun, X.; Sartipi, S.; Kapteijn, F.; Gascon, J. Effect of pretreatment atmosphere on the activity and selectivity of Co/meso HZSM-5 Fischer-Tropsch synthesis. *New J. Chem.* **2016**. [CrossRef]

8. Akay, G. Process Intensification in the Catalytic Synthesis of Supported Catalysts with Hierarchic Pore Structure. WIPO Patent Application WO/2013/108045, 25 July 2013.
9. Bakker, M.; Sayler, F.M.; Grano, A.; Smatt, J.-H. Methods for Preparing and Using Metal and/or Metal Oxide Porous Materials. U.S. Patent 8,574,340, 5 November 2013.
10. Coppens, M.-O. A nature inspired approach to reactor and catalysis engineering. *Curr. Opin. Chem. Eng.* **2012**, *1*, 281–289. [CrossRef]
11. Gascon, J.; van Ommen, J.R.; Moulijn, J.A.; Kapteijn, F. Structuring catalyst and reactor—An inviting avunue to process intensification. *Catal. Sci. Technol.* **2015**, *5*, 807–817. [CrossRef]
12. Akay, G.; Calkan, B. Preparation of nanostructured microporous metal foams through flow induced electroless deposition. *J. Nanomat.* **2015**, *2015*, 275705. [CrossRef]
13. Mostafid, A.M. Entrance and Exit Effects on Flow through Metallic Foams. Ph.D. Thesis, Concordia University, Montreal, QC, Canada, 2007.
14. Akay, G.; Birch, M.A.; Bokhari, M.A. Microcellular polyHIPE polymer supports osteoblast growth and bone formation *in vitro*. *Biomaterials* **2004**, *25*, 3991–4000. [CrossRef] [PubMed]
15. Akay, G.; Burke, D.R. Agro-process intensification through synthetic rhizosphere media for nitrogen fixation and yield enhancement in plants. *Am. J. Agric. Biol. Sci.* **2012**, *7*, 150–172.
16. Akay, G.; Pekdemir, T.; Shakorfow, A.M.; Vickers, J. Intensified demulsification and separation of thermal oxide reprocessing interfacial crud (THORP-IFC) simulant. *Green Process. Synth.* **2012**, *1*, 109–127. [CrossRef]
17. Akay, G. Bioprocess and chemical process intensification. In *Encyclopedia of Chemicals Processing*; Lee, S., Ed.; Taylor and Francis: New York, NY, USA, 2006; Volume 1, pp. 183–199.
18. Vriezema, D.M.; Aragones, M.C.; Elemans, J.A.A.W.; Cornelissen, J.J.L.M.; Rowan, A.E.; Nolte, R.J.M. Self-assembled nanoreactors. *Chem. Rev.* **2005**, *105*, 1445–1490. [CrossRef] [PubMed]
19. Osterloh, F.E. Inorganic nanostructures for photoelectrochemical and photocatalytic water splitting. *Chem. Soc. Rev.* **2013**, *42*, 2294–2320. [CrossRef] [PubMed]
20. Johnson, R. Catalysis in compartments. *Nat. Chem.* **2014**, *6*, 5. [CrossRef]
21. Bain, J.; Staniland, S.S. Bioinsprired nanoreactors for the biomineralisation of metallic-based nanoparticles for nanomedicine. *Phys. Chem. Chem. Phys.* **2015**, *17*, 15508–15521. [CrossRef] [PubMed]
22. Akay, G.; Tong, L. Preparation of low density polyethylene latexes by flow induced phase inversion emulsification of polymer melt in water. *J. Colloid Interface Sci.* **2001**, *239*, 342–357. [CrossRef] [PubMed]
23. Miller, R.; Ferri, J.K.; Javadi, A.; Kragei, J.; Mucic, N.; Wustneck, R. Rheology of interfacial layers. *Colloid Polym. Sci.* **2010**, *288*, 937–950. [CrossRef]
24. Langford, J.I.; Wilson, A.J.C. Scherrer after sixty years: A survey and some new results in the determination of crystallite size. *J. Appl. Cryst.* **1978**, *11*, 102–113. [CrossRef]
25. Ahmad Monshi, A.; Foroughi, M.R.; Monshi, M.R. Modified Scherrer equation to estimate more accurately nano-crystallite size using XRD. *World J. Nano Sci. Eng.* **2012**, *2*, 154–160. [CrossRef]
26. Akay, G.; Dissanayake, B.; Morgan, A. Process intensification in particle technology: Production of powder coatings produced by non-isothermal flow-induced phase inversion. *Ind. Eng. Chem. Res.* **2011**, *50*, 3239–3246. [CrossRef]
27. Akay, G. Flow induced phase inversion in the processing of concentrated emulsions. *Chem. Eng. Sci.* **1998**, *52*, 203–223. [CrossRef]
28. Malkin, A.Y.; Isayev, A.I. *Rheology: Concepts, Methods, and Applications*; ChemTech Publishing: Toronto, Canada, 2006.
29. Peng, Y.; Chen, W.; Ficher, T.M. Short-time self-diffusion of nearly hard spheres at an oil-water interface. *J. Fluid Mech.* **2009**, *618*, 243–261. [CrossRef]
30. Reynaert, S.; Moldenaers, P.; Vermant, J. Interfacial rheology of stable and weakly aggregated two-dimensional suspensions. *Phys. Chem.* **2007**, *9*, 6463–6475. [CrossRef] [PubMed]
31. Fanning, J.C. The chemical reduction of nitrate in aqueous solution. *Coord. Chem. Rev.* **2000**, *199*, 159–179. [CrossRef]
32. Binks, B.; Lumsdon, S. Influence of particle wettability on the type and stability of surfactant-free emulsions. *Langmuir* **2000**, *16*, 8622–8631. [CrossRef]
33. Binks, B.; Kirkland, M. Interfacial structure of solid-stabilized emulsions studied by scanning electron microscopy. *Phys. Chem. Chem. Phys.* **2002**, *4*, 3727–3733. [CrossRef]

34. Garrett, P.R. *The Science of Defoaming: Theory, Experiment and Applications*; CRC Press: New York, NY, USA, 2013.
35. Khoukh, S.; Perrin, P.; Berc, F.B.D.; Tribet, C. Reversible light-triggered control of emulsion type and stability. *ChemPhysChem* **2005**, *6*, 2009–2012. [CrossRef] [PubMed]
36. Tabor, R.F.; Pottage, M.J.; Garvey, C.J.; Wilkinson, B.L. Light-induced structural evolution of photoswitchable carbohydrate-based surfactant micelles. *Chem. Commun.* **2015**, *51*, 5509–5512. [CrossRef] [PubMed]
37. Khedr, M.H.; Halin, K.S.A.; Soliman, N.K. Synthesis and photocatalytic activity of nano-sized iron oxides. *Mater. Lett.* **2009**, *63*, 598–601. [CrossRef]
38. Murakami, N.; Matsuo, T.; Tsubota, T.; Ohno, T. Photocatalytic reaction over iron hydroxides: A novel visible-light-responsive photocatalyst. *Catalal. Commun.* **2011**, *12*, 341–344. [CrossRef]
39. Wieczorek, K.; Kozak, A.J. The thermal decomposition of $Fe(NO_3)_3 \cdot 9H_2O$. *J. Therm. Anal. Calorim.* **1999**, *58*, 647–651. [CrossRef]
40. Malecki, A.; Gajerski, R.; Lubus, S.; Prochowska-Klisch, B.; Wojciechowski, K.T. Mechanism of the thermal decomposition of d-metal nitrates hydrates. *J. Therm. Anal. Calorim.* **2000**, *60*, 17–23. [CrossRef]
41. Brockner, W.; Ehrhardt, C.; Gjikaj, M. Thermal decomposition of nickel nitrate hexahydrate, $Ni(NO_3)_2 \cdot 6H_2O$, in comparison to $Co(NO_3)_2 \cdot 6H_2O$ and $Ca(NO_3)_2 \cdot 4H_2O$. *Thermochim. Acta* **2007**, *456*, 64–68. [CrossRef]
42. Malacka, B.; Lacz, A.; Drozdz, E.; Malecki, A. Thermal decomposition of d-metal nitrates supported on alumina. *J. Therm. Anal. Calorim.* **2015**, *119*, 1053–1061. [CrossRef]
43. Akay, G. Flow induced phase inversion agglomeration: Fundamentals and batch processing. *Polym. Eng. Sci.* **1994**, *34*, 865–880. [CrossRef]
44. Akay, G.; Tong, L.; Addleman, R. Process intensification in particle technology: Intensive granulation of powders by thermo-mechanically induced melt fracture. *Ind. Eng. Chem. Res.* **2002**, *41*, 5436–5446. [CrossRef]
45. Akay, G.; Harrasi, W.S.S.; El Naggar, A.M.A.; Mohamed, A.H.; Zhang, K. Integrated Intensified Biorefinery for Gas-to-Liquid Conversion. European Patent Application EP2837423, 18 February 2015.
46. Akay, G. Ammonia Production by Integrated Intensified Processes. WIPO Patent Application WO/2012/025767, 1 March 2012.
47. Harrasi, W.S.S.; Zhang, K.; Akay, G. Process intensification in gas-to-liquid reactions: Plasma promoted Fischer-Tropsch synthesis for hydrocarbons at low temperatures and ambient pressure. *Green Process. Synth.* **2013**, *2*, 479–490.
48. Buurmans, I.L.C.; Weckhuysen, B.M. Heterogeneties of individual catalyst particles in space and time as monitored by spectroscopy. *Nat. Chem.* **2012**, *4*, 873–886. [CrossRef] [PubMed]
49. Saiz, E.; Goldman, M.; Gomez-Vega, J.M.; Tomsia, A.P.; Marshall, G.W.; Marshall, S.J. *In vitro* behavior of silicate glass coatings on Ti6A14V. *Biomaterials* **2002**, *23*, 3749–3756. [CrossRef]
50. Chica, A.; Sayas, S. Effect and stable bioethanol steam reforming catalyst based on Ni and Co supported on all-silica delaminated ITQ-2 Zeolite. *Catal. Today* **2009**, *146*, 37–43. [CrossRef]
51. Sarkar, A.; Tirumkudulu, M.S. Delamination of drying nanoparticle suspensions. *Soft Matter* **2011**, *7*, 8816–8822. [CrossRef]
52. Guadagnino, E.; Zuccato, D. Delamination propensity of pharmaceutical glass containers by accelerated testing with different extraction media. *J. Pharm. Sci. Technol.* **2012**, *66*, 116–125. [CrossRef] [PubMed]
53. Akay, G.; Wakeman, R.J. Crossflow Microfiltration Behaviour of a Double Chain Surfactant Dispersion in Water—I: The Effect of Process and Membrane Characteristics on Permeate Flux and Surfactant Rejection. *Chem. Eng. Sci.* **1994**, *49*, 271–283. [CrossRef]
54. Laughlin, R.G. *The Aqueous Phase Behaviour of Surfactants*; Academic Press: London, UK, 1996.
55. De Gennes, P.G.; Prost, J. *The Physics of Liquid Crystals*; Clarendon Press: Oxford, UK, 1993.